Secreted inhibitors drive the loss of regeneration competence in *Xenopus* limbs

Can Aztekin[1,2]*, Tom W. Hiscock[1,3,4]*, John Gurdon[1,2], Jerome Jullien[1,2,5]† John Marioni[3,6,7]†, Benjamin David Simons[1,8,9]†

AFFILIATIONS

[1] Wellcome Trust/Cancer Research UK Gurdon Institute, University of Cambridge, Cambridge, UK.

[2] Department of Zoology, University of Cambridge, Cambridge, UK.

[3] Cancer Research UK Cambridge Institute, University of Cambridge, Cambridge, UK.

[4] Institute of Medical Sciences, Foresterhill Health Campus, University of Aberdeen, Aberdeen AB25 2ZD Scotland, UK

[5] Nantes Université, Inserm, Centre de Recherche en Transplantation et Immunologie, UMR 1064, ITUN, F-44000 Nantes, France

[6] EMBL–European Bioinformatics Institute, Wellcome Genome Campus, Cambridge, UK.

[7] Wellcome Sanger Institute, Wellcome Genome Campus, Cambridge, UK.

[8] Department of Applied Mathematics and Theoretical Physics, Centre for Mathematical Sciences, University of Cambridge, Cambridge, UK.

[9] Wellcome Trust Centre for Stem Cell Research, University of Cambridge, Cambridge, UK.

*Co-first authors.

†Corresponding authors; listed in alphabetical order.

Correspondence to: jerome.jullien@inserm.fr (J.J); marioni@ebi.ac.uk (J.C.M); bds10@cam.ac.uk (B.D.S.)

Keywords: limb regeneration, Xenopus, apical-ectodermal-ridge, scRNA-Seq, ex vivo limbs

One sentence summary: Secreted inhibitors associated with chondrogenic progression inhibit AER cell formation and restrict limb regeneration potential.

ABSTRACT

Absence of a specialized wound epidermis is hypothesized to block limb regeneration in higher vertebrates. However, the factors preventing its formation in regeneration-incompetent animals are poorly understood. To characterize the endogenous molecular and cellular regulators of specialized wound epidermis formation in *Xenopus laevis* tadpoles, and the loss of their regeneration-competency during development, we used single-cell transcriptomics and *ex vivo* regenerating limb cultures. Transcriptomic analysis revealed that the specialized wound epidermis is not a novel cell state, but a re-deployment of the apical-ectodermal-ridge (AER) program underlying limb development. Enrichment of secreted inhibitory factors, including *Noggin*, a morphogen expressed in developing cartilage/bone progenitor cells, are identified as key inhibitors of AER cell formation in regeneration-incompetent tadpoles. These factors can be overridden by *Fgf10*, which operates upstream of *Noggin* and blocks chondrogenesis. These results indicate that manipulation of the extracellular environment and/or chondrogenesis may provide a strategy to restore regeneration potential in higher vertebrates.

INTRODUCTION

Amphibian limb regeneration relies on a specialized wound epidermis (also known as the apical-epithelial-cap, AEC) that forms on the amputation plane and has been characterized primarily as a tissue in regenerating salamander limbs (Campbell et al., 2011; Campbell and Crews, 2008; Knapp et al., 2013, p. 2013; Monaghan et al., 2012; Pearl et al., 2008; Tsai et al., 2020, 2019). It has been hypothesized that the absence or immature state of this tissue limits the regeneration potential of higher vertebrates, including mammals (Tassava & Olsen, 1982). The AEC has been suggested to impact underlying tissues by: degrading extracellular matrix (Kato et al., 2003; Miyazaki et al., 1996; Yang et al., 1999); secreting growth factors to promote proliferation (Han et al., 2001; Thornton, 1960; Thornton and Thornton, 1965; Tsai et al., 2020); enabling the self-renewal of underlying progenitor and dedifferentiated cells, leading to the formation of a proliferative structure called the blastema (Mescher, 1976; Tassava and Loyd, 1977; Tassava and Mescher, 1975); and providing directionality cues for growth (Ghosh et al., 2008; Thornton, 1960; Thornton and Thornton, 1965). Some marker genes associated with AEC (*e.g. Fgf8, Fn1*) were specifically seen only in the basal layers of AEC tissue, suggesting there is cellular heterogeneity within the AEC (Christensen and Tassava, 2000; Tsai et al., 2020; Yokoyama et al., 2000). However, it remains largely unclear which cell types within AEC *tissue* are critical for regeneration, which transcriptional and functional properties are associated with a mature AEC and regeneration, and why the AEC cannot form or maturate in some instances/species.

Due to their requirement for proximal-distal outgrowth as well as the similarity in *Fgf8* expression patterns, the AEC in regenerating limbs was suggested to be analogous to the apical-ectodermal-ridge (AER), a tissue that has been well-studied during mouse and chicken limb development (Beck et al., 2009). However, current results suggest that limb regeneration-competent salamanders lack a developmental AER (Purushothaman et al., 2019). Moreover, recent findings (including single-cell transcriptomic data) have provided conflicting results on epidermal *Fgf8* expression during axolotl limb regeneration (Gerber et al., 2018; Han et al., 2001; Leigh et al., 2018; Li et al., 2020; Nacu et al., 2016; Qin et al., 2020; Rodgers et al., 2020; Vincent et al., 2020). Therefore, it is unclear if cells within AEC tissue use a novel transcriptional programme for regeneration, or whether they re-deploy a transcriptional programme associated with developmental AER.

Xenopus laevis is the only commonly used model organism that develops their limbs in a similar manner to amniotes, has a detectable AER, and shows limb regeneration ability (Purushothaman et al., 2019). Moreover, tadpoles lose their limb regeneration ability progressively during development, coinciding with their inability to form a specialized wound epidermis, although the mechanisms of regeneration incompetence and their connection to the specialized wound epidermis remain incompletely understood (Christen & Slack, 1997; Dent, 1962). At the developmental stages prior to the formation of digits, amputations lead to a complete regeneration of the limb (Niewkoop and Faber, NF (Nieuwkoop and Faber, 1994) ~52-54, regeneration-competent). As autopod development proceeds, amputations result in partial regeneration, characterized by missing digits (NF ~55-57, regeneration-restricted). Towards metamorphosis, amputations either cause the growth of an unpatterned spike-like cartilaginous structure without joints and muscles, or a simple wound healing response (NF ~58 and beyond, regeneration-incompetent) (Beck et al., 2009; Dent, 1962). In addition to being stage-dependent, *Xenopus* limb regeneration competence depends on amputation position, and is reduced when amputations are performed at more proximal regions of the limb, where there are more mature chondrogenic and osteogenic cells (Nye & Cameron, 2005; Wolfe et al., 2000). Likewise amputation through bone results in reduced regeneration compared to amputations at the joints (Nye & Cameron, 2005; Wolfe et al., 2000). Nonetheless, it remains unclear what is the association of this stage- and position-dependence with regeneration competency.

Regeneration-incompetency was suggested to result from changes in mesodermal tissue, and may involve defects in patterning of the blastema (Sessions and Bryant, 1988; Yokoyama et al., 2001). In particular, the lack of activating signals (e.g. *Fgf10*) was proposed to prevent the formation of a specialized wound epidermis (Yokoyama et al., 2001). However, these studies were performed at the tissue-level, and it remains unclear which individual cell types within the tissue are responsible for regeneration-incompetency, whether intrinsic properties of mesodermal cell types fail to activate upon injury, and if there is a role of inhibitory secreted factors, rather than a lack of activating factors, in determining regeneration-outcome. Additionally, exogenous perturbations to major signaling pathways (e.g. BMP (Beck et al., 2006; Pearl et al., 2008), FGF (D'Jamoos et al., 1998), WNT (Yokoyama et al., 2011)) were shown to inhibit regeneration. However, it is largely unknown how these pathways

endogenously influence cell types and cellular behaviors during regeneration, or how these different pathways operate in the context of cell-cell interactions mediating regeneration. Overall, whilst there are numerous tissues and genes implicated in limb regeneration competency, there is currently no unifying cellular model accounting for these disparate observations.

Here, by using single-cell RNA-sequencing (scRNA-seq), we define the cellular framework of specialized wound epidermis formation during regeneration and its failure to form at later developmental stages. Then, by using scRNA-seq and *ex vivo* limb cultures, we revealed the critical role of secreted inhibitory factors in determining regeneration-competency, and tested this phenotype by using regeneration associated genes. Together, these findings implicate a cellular mechanism in which factors secreted during bone/cartilage formation inhibit the formation of specialized wound epidermis at later developmental stages, compromising regeneration competency.

RESULTS

Single-cell RNA-seq analysis reveals cell type heterogeneity during development and following amputation of the limb

To compare differences in AER and AEC, as well as to detail the cellular landscape of regeneration, we utilized single-cell transcriptomics. To characterize developmental AER and cellular changes associated with regeneration ability, we first sequenced developing intact hindlimbs at specific morphologically-defined stages: NF Stage ~52 (limb bud stages), NF Stage ~54 (autopod forming) and NF Stage ~56 (autopod formed) **(Figure 1A)**. Then, to evaluate regeneration-associated AEC and the cellular responses to amputations, we profiled cells from amputated limbs and their contralateral controls. Specifically, we amputated hindlimbs from presumptive knee/ankle levels for regeneration-competent tadpoles (NF Stage ~52-53) and ankle level for –restricted (NF Stage ~55-56) and –incompetent tadpoles (NF Stage ~58-60), and sequenced cells from newly-generated tissues at 5 days post-amputation (dpa) **(Figure 1B)** when the specialized wound epidermis and blastema are seen morphologically (Beck et al., 2009). Contralateral developing limb buds or autopods were sequenced as controls. We did not include a contralateral control at the regeneration-

incompetent stage as our dissociation protocol was unable to dissociate bone cells without compromising other tissues.

Next, we pooled the single-cell RNA sequencing data derived from at least two replicates for each condition **(Figure S1),** and corrected our atlas for cell cycle effects **(Figure S2)**, yielding a total of 42,348 cells **(Materials and Methods; Figures 1C-D; Figure S3-4; Supplementary Table 1**). Following clustering of cells based upon their gene expression profiles, examination of multiple marker genes **(Figure S5)** revealed at least 60 distinct clusters representative of putative cell types **(Figures 1C and S3)**, including known populations (e.g. AER cells) and potentially new and uncharacterized cell states (e.g. a *Piwil1*+ population in the mesenchyme) **(Figure 1E)**. From the cell atlas, we were able to detect cell cycle differences between cell types, e.g. distal mesenchyme progenitors were more biased towards G2/M phases compared to proximal mesenchyme progenitors **(Figure S2)**, as reported in mouse (Boehm et al., 2010). The *Xenopus* limb cell atlas is accessible using an interactive platform (https://marionilab.cruk.cam.ac.uk/XenopusLimbRegeneration/).

Quantitative features of AER cell formation are associated with regeneration outcome

We then focused on the specialized wound epidermis, or AEC, that was suggested to be analogous to the AER. Although both populations were characterized by *Fgf8* expression (Beck et al., 2009), the extent of similarity between these cells was not previously tested beyond assessing similarity of expression for a small number of markers. Using our single-cell atlas, we compared the transcriptional profiles of cells that belonged to the AER (defined as *Fgf8* expressing epidermal cells during limb development) and the AEC (*Fgf8* expressing epidermal cells in 5 dpa samples). Whilst we did see some quantitative expression differences between cells related to AEC and AER tissues (**Figure S5, S6A, Supplementary Table 2**), they expressed many genes in common and showed a high degree of transcriptional similarity (**Figures 2A-B, S5**). Consistent with this, cells related to these tissues were aggregated within a single *Fgf8*+ epidermal cluster **(Figures 2B-C)**. Additionally, both during development and 5 days post-amputation, *Fgf8*+ epidermal cells were mostly detected as a monolayer of polarized cuboidal basal cells **(Figure S7)**, though multilayers were seen to form in some instances **(Figure S8)**. This suggests that AEC and AER *tissues* are not homogenous in their cellular composition, and that it is only the basal cells that express the key *Fgf8*+

transcriptional program. Overall, based on their transcriptomic signature, tissue localization, and cellular morphology, the *Fgf8+* cells that compose the AEC and AER tissues are very similar. We find that the AEC tissue does not require a novel cell state, but rather a re-deployment of the transcriptional program associated with developmental AER, albeit with a higher signaling center potential (**Figure 2E, S6C-D)**. Due to their high-degree of similarity and common expression of developmental AER genes, we named all cells from the identified *Fgf8+* epidermal cluster as *AER cells*, and referred to specific samples to distinguish between cells from the regeneration-associated AEC and the developmental AER.

To test the similarities of cell types composing the specialized wound epidermis in different regeneration conditions, we compared transcriptomes of cells corresponding to limb and tail specialized wound epidermis. We found that AER cells (limb specialized wound epidermal cells) and cells that define the specialized wound epidermis during *Xenopus* tail regeneration (regeneration-organizing-cells, ROCs (Aztekin et al., 2019)) showed similar, but non-identical gene expression profiles **(Figure S9)**, emphasizing that the cellular framework of the specialized wound epidermis is context-dependent and appendage regeneration scenarios can utilize different cell types.

Limb amputation is known to result in the formation of *Fgf8* expressing AEC at the amputation plane in regeneration–competent tadpoles, but not in regeneration–incompetent tadpoles (Christen & Slack, 1997), while AEC formation has not been characterized previously for regeneration–restricted tadpoles. Using our atlas, we found that, at 5 dpa, tadpole epidermis contained abundant AER cells in regeneration–competent tadpoles and a limited number of AER cells in regeneration-restricted tadpoles, while AER cells were largely absent from regeneration-incompetent tadpoles **(Figures 2B-D)**. In parallel, AER cell associated ligand expressions were lower or absent in regeneration-incompetent *tp63+* epidermal cells **(Figure S6E)**. In our dataset, we found that different populations express ligands from different major signalling pathways (FGF, BMP, WNT, DELTA, TGFB) **(Figures S6C)**. However, only AER cells can express multiple ligands from these gene families altogether and at a very high level, making them a highly potent signalling centre **(Figures 2E, S6)**. Although *Fgf8* was always expressed in AER cells, the relative expression of *Fgf8* and other ligands varied among conditions **(Figure 2E, S6, Supplemental Table 2)**, emphasizing that the detection of *Fgf8* alone does not discriminate the signaling center potency of AER cells. Indeed, in addition to the changes in AER cell abundance, we also

detected differentially expressed genes between AER cells from regeneration-competent and –restricted tadpoles **(Figure S6B)**. These differences suggest that AER cells in regeneration-competent 5 dpa samples may be more "mature" compared to regeneration-restricted ones, although further work on the functional role of these genes is required. Overall, while the signaling center potency of AER cells appeared variable, the redeployment of this developmental cell type with a high signaling center potential had a strong correlation with regeneration-outcome.

The presence of AER cells is associated with injury-induced mesenchymal plasticity

It has been suggested that the AEC enables the self-renewal activity of dedifferentiated cells, leading to blastema formation (Tassava & Mescher, 1975; Tassava & Loyd, 1977). To identify signatures of dedifferentiation in our atlas, we first examined the expression of genes related to dedifferentiation and blastema formation (Gerber et al., 2018; Haas and Whited, 2017; Leigh et al., 2018) (e.g. *Sall4*, *Kazald1*). We found that these genes were either already expressed before amputation or upregulated upon amputation in a subset of fibroblasts **(Figures S10A-B)** that were located near the skin and perichondrium **(Figure S11)**. Likewise, we found that a small fraction of these fibroblasts expressed muscle-related genes (e.g. *Pax3*) before and after amputation **(Figure S10B)**. Moreover, independent of regeneration-outcome, amputation resulted in these fibroblast cells expressing genes related to distal mesenchyme progenitors (e.g. *Grem1, Shh, Msx1, Fgf10*) and chondrogenesis (e.g. *Col8a2, Sox9)* **(Figure S10A)**. Lastly, amputation not only increased the expression of known marker genes, but also led to the up-regulation of an entire putative distal mesenchyme progenitor gene set **(Figure S10C)**, with the magnitude of this up-regulation being lower in samples having fewer AER cells. Together, we concluded that, upon amputation, a subset of fibroblasts manifest injury-induced mesenchymal plasticity - at least at the transcriptional level - and its extent correlates with AER cell abundance.

AER cell formation requires activation of multiple signaling pathways

To investigate the molecular mechanisms that mediate AER cell formation upon amputation, we developed an *ex vivo* regenerating limb culture protocol, inspired by previous work (Cannata et al., 1992) **(Figure 3A)**. By culturing amputated stylopod, or zeugopod and stylopod from regeneration-competent and regeneration–restricted tadpoles, respectively, we

observed *Fgf8* cell formation at the distal part of explants within 3 dpa (**Figure 3B**). Regeneration-competent explants also exhibited cone-shaped growth as cells accumulated uniformly underneath *Fgf8* cells, mimicking *in vivo* regeneration **(Figures 3A-B, and S12A-B)**. Interestingly, the proximal region of explants was also covered with epidermis **(Figure S12A, and S13A)**, but neither *Fgf8* expressing cells nor a uniform cell accumulation underneath the epidermis was observed **(Figures 3A-B, S12B, and S13A)**. Moreover, the proximal part of the explant exhibited active chondrogenesis, manifesting in an outwards growth of cartilaginous tissue **(Figures 3A and S12C)**. This phenotype was particularly pronounced when explants were harvested from developmental stages in which proximal tissues were advanced in chondrogenesis (onset of NF Stage 53-54) **(Figures 3A and S12D)**, and could be further enhanced by addition of BMP4, a known chondrogenesis inducer **(Figure S12E)**. Hence, the proximal and distal sites of limb explants exhibit different behaviors: the distal sites recapitulate localized AER cell formation as seen *in vivo*, while the proximal site is characterized by active chondrogenesis without AER cell formation.

In addition to changes associated with regeneration, explants could be used to determine signaling requirements for specialized wound epidermis formation. Inhibition of FGF, BMP, and WNT pathways via small molecule inhibitors blocked AER cell formation in explants **(Figure 3C)**, reinforcing the conclusion that the *in vivo* AEC effects reported in former studies are mediated through a direct effect on the limb rather than a systemic effect (Beck et al., 2006; D'Jamoos et al., 1998; Yokoyama et al., 2011). Moreover, by using the culture assay, we found that active TGF-β and NOTCH signaling are also required for *Xenopus* AER cell formation **(Figure 3C)**. Overall, we concluded that AER cell formation requires the activity of multiple major signaling pathways, although further work is required to determine what roles these pathways play and whether they directly or indirectly regulate AER cell formation.

AER cells can form without cell division

Next, we asked how AER cells form on the amputation plane. It has been suggested that salamander AEC tissue forms by migration of epidermal cells to the amputation plane, and may not require cell proliferation (Campbell and Crews, 2008; Hay and Fischman, 1961). Moreover, the mouse AER was previously suggested to be a largely mitotically inactive tissue (Storer et al., 2013). However, it is not known whether similar mechanisms apply to

AER cells within the specialised wound epidermis, and also to what extent they are seen in *Xenopus.* Therefore, we first traced skin tissue located on the edge of explants, and found that they contributed to the covering of both the distal and proximal sites **(Figure S13B)**. As the amputation planes are covered by skin tissue from the surrounding area, we reasoned that AER cells are likely to have originated from skin cells. As amputation eliminates the majority, if not all, of AER cells in the limb, we hypothesized that AER cells are derived from remaining skin stem cells. If AER cells are induced through proliferation and differentiation following amputation, all AER cells should be the product of cell division. To test this hypothesis, we assayed the level of EdU incorporation (labelling newly synthesized DNA, hence divided cells) in newly-formed AER cells, using *Fgf8* positivity to specifically identify AER cells within the AEC tissue. We found that only ~40% of AER cells (distal epidermal *Fgf8+*) were EdU positive at 3 dpa **(Figure S13C)**, suggesting that most AER cells are induced independently of cell division following amputation. These results parallel our transcriptomics-based cell-cycle assessment in which AER cells display low levels of proliferation **(Figure S2D)**. Using the transcriptomics data, we identified a stepwise activation of *Lgr5.S* (a WNT target gene) followed by *Fgf8.L* expression as a possible gene-expression trajectory that could allow basal epidermal cells to convert directly to AER cells without cell division (**Figure 3D)**. Consistent with such a process, when visualized *in vivo*, we found that *Fgf8+/Lgr5+* AER cells were flanked by *Lgr5+* cells in the basal epidermis on the amputation plane or in the developing limb **(Figures 3E and S7A-B)**. Overall, these results support the hypothesis that basal epidermal cells can acquire AER cell identity without cell division, although understanding the functional relevance of cell division on AER cell fate requires further work.

Loss of regeneration potential is associated with enrichment in inhibitory secreted factors to AER cell formation

We then asked why fewer or, respectively, no AER cells form on the amputation plane of regeneration-restricted or -incompetent tadpoles. Previous studies have proposed that lack of activating signals in the mesodermal tissue, specifically *Fgf10*, causes regeneration-incompetency (Yokoyama et al., 2001). However, these results cannot explain why regeneration is impaired when amputations are conducted through bone or at more proximal limb regions, nor why the proximal site of limb explants cannot form AER cells. Thus, we assessed whether *Fgf10* can induce *Fgf8* expression across the whole epidermis or whether

there are additional requirements for distal epidermal *Fgf8* expression, and hence AER cell formation.

When we examined the spatial correlation between *Fgf10.L* expressing mesenchymal cells and *Fgf8.L* expressing epithelial cells in regeneration–competent tadpoles, we saw regions in which *Fgf10.L* but not *Fgf8.L* was present **(Figure S14A)**. Second, when adding FGF10 to regeneration–competent explants, we observed a slight, but not statistically significant, increase in AER cell formation on the amputation plane **(Figure S14B)**; although this signal was confined to the distal epidermis and did not include a substantial signal at the proximal site of explants **(Figure S14C)**, where chondrogenic populations are more abundant. This suggested that FGF10 alone cannot induce AER formation across the entire epidermis, and that the presence/absence of further activating/inhibitory signals are involved in AER cell formation.

To test whether there are inhibitory factors secreted from regeneration-incompetent tadpole limbs that block AER cell formation, we took advantage of our *ex vivo* cultures. First, we co-cultured *ex vivo* limbs from regeneration-competent and –incompetent tadpoles. Strikingly, when such cultures were stained against *Fgf8* at 3 dpa, we observed that regeneration-competent tadpole limbs failed to form AER cells **(Figure 4A**). Second, we collected media from regeneration-incompetent tadpole explants and cultured freshly amputated regeneration-competent explants with this conditioned media. Consistent with the co-culture experiment, the conditioned media from regeneration-incompetent tadpoles blocked AER cell formation in regeneration-competent explants **(Figure 4B)**. By contrast, neither co-culturing with regeneration–competent explants, nor preparing conditioned media from regeneration-competent explants, affected AER cell formation in regeneration–competent explants **(Figure 4A-B)**. Additionally, conditioned media from regeneration–competent explants was unable to induce AER cell formation in regeneration–incompetent explants **(Figure S15A-B)**, emphasizing that it is the enrichment of inhibitory secreted factors that is the dominant process interfering with AER cell formation, rather than a depletion in regeneration-promoting factors. Altogether, these results suggest that secreted inhibitory factors block AER cell formation in regeneration-incompetent tadpoles, presumably compromising their regeneration potential.

To identify the factors responsible for this inhibitory effect, we surveyed our single-cell atlas for the expression of secreted proteins involved in signaling pathways required for AER cell formation. We found that that the loss of regeneration potential is associated with an increased proportion of chondrogenic lineage cells in the mesenchyme **(Figure 4C**, aligning with previous tissue-level observations (Dent, 1962)) and that these cells express multiple inhibitory ligands for BMP and WNT pathways **(Figure 4D)**. As chondrogenic populations specifically express high levels of *Noggin* **(Figure 4D)**, a known antagonist of BMP signaling, we hypothesized that AER cell formation is antagonized by an excess of secreted *Noggin* in regeneration-incompetent tadpoles. Indeed, consistent with previous observations (Pearl et al., 2008), addition of NOGGIN to regeneration-competent *ex vivo* limbs blocked AER cell formation **(Figure S15C)**. To test whether endogenous *Noggin* does indeed act as one of the inhibitory secreted factors produced following amputation in regeneration-incompetent tadpoles, we blocked NOGGIN in our co-culture and conditioned media experiments using anti-NOGGIN antibodies **(Figure 4A-B)**. Strikingly, blocking secreted NOGGIN by antibody addition cancelled the inhibitory activity on AER cell formation in both co-culture and conditioned media experiments **(Figure 4A-B)**. Based on these observations, we then explored whether anti-NOGGIN application would improve the *in vivo* amputation response. Indeed, when beads loaded with anti-NOGGIN antibodies were implanted on the amputation plane of regeneration-restricted/incompetent tadpoles, we saw a mild improvement in the regenerative response **(Figure 5A)**, highlighting that secreted inhibitors are influencing the regeneration-outcome *in vivo*.

As these experiments point towards the chondrogenic lineage as the source of inhibitory secreted factors, we then asked if limiting chondrogenesis can promote AER cell formation. To this end, we generated tip explants by culturing distal limb buds (NF Stage ~52) or early formed autopods (NF Stage ~54) without their proximal segment, where the most advanced chondrogenesis takes place. Indeed, these tip explants showed ectopic *Fgf8* expression at different sites of the epidermis further suggesting a localized and/or long-range inhibitory effect of secreted factors from mature chondrogenic cells (**Figure S15D)**. Moreover, the inability of the proximal explant epidermis to form AER might be explained, at least in part, by the abundance of chondrogenic cells at the proximal site **(Figure 3A-B)**. Overall, these results indicate that the loss of AER cell formation ability is associated with an enrichment in inhibitory secreted factors, including NOGGIN, that are secreted primarily from the chondrogenic lineage.

As NOGGIN is known to neutralize secreted BMPs, we then focused on assessing the effect of the BMP pathway on AER cell formation. Previously, it was demonstrated that, not only do mouse and chicken AER require active BMP signaling, but also that excess BMP activation abolishes AER (Pajni-Underwood et al., 2007; Pizette et al., 2000.; Pizette & Niswander, 1999; Verheyden & Sun, 2008). To test whether manipulation of BMP signaling can also impact *Xenopus* AER cell formation in regeneration–competent tadpoles, we perturbed the BMP pathway. We found that the addition of BMP4 to regeneration–competent *ex vivo* cultures blocked AER cell formation **(Figure S15C)**, an effect similar to that reported in chick and mouse embryos (Pajni-Underwood et al., 2007; Pizette et al., 2000; Pizette and Niswander, 1999; Verheyden and Sun, 2008). The addition of NOGGIN to regeneration–competent *ex vivo* cultures blocked AER cell formation **(Figure S15C)**, as reported before *in vivo* (Beck et al., 2006; Jones et al., 2013). Moreover, we found that inhibiting NOGGIN could increase the formation of AER cells **(Figure S15C)**, suggesting endogenous BMP4 levels do not reach a level where AER cell formation is blocked. As BMP4 boosts chondrogenesis **(Figure S12E)**, which can in turn lead to *Noggin* expression, these results suggest that fine tuning of BMP agonist and antagonists levels in the growing limb are key for AER cell formation.

FGFR activation negatively regulates progression of chondrogenesis and FGF pathway operates upstream of NOGGIN for AER cell formation

As regeneration competency in late stage tadpoles was shown previously to be restored via exogenous application of FGF10 (Yokoyama et al., 2001), we next sought to evaluate whether the effect of *Fgf10* on regeneration is, at least in part, mediated by its impact on chondrogenesis and *Noggin* expression. To test the effect of *Fgf10* on chondrogenesis, we used our *ex vivo* cultures to monitor the substantial chondrogenesis occurring at the proximal site of explants. Application of FGF10 beads to the proximal site of *ex vivo* cultures, or addition of recombinant FGF10 to their media, significantly decreased chondrogenesis at the proximal sites in regeneration-restricted explants **(Figure 5B)**. Conversely, blocking FGFR significantly extended chondrogenesis at the proximal site of explants **(Figure 5C-D, Figure S16)**. Nonetheless, FGF10 treatment was not sufficient to induce strong Fgf8 expression at the proximal site of explants **(Figure S14C)**, which we hypothesize could be, at least in part, attributable to differences in the abundance of proposed antagonist cues. To test this

hypothesis, we treated explants with a combination of FGF10 and anti-NOGGIN antibodies. Strikingly, this combination not only enhanced AER cell formation at the distal sites, but also induced ectopic *Fgf8.L* expression near the proximal sites of explants **(Figure 5E-F)**, further suggesting that the enrichment of inhibitory secreted factors from the chondrogenic lineage affect the ability to form AER cells. Lastly, AER cell formation induced by FGF10 addition was cancelled by the addition of BMP inhibitors (NOGGIN or small molecule inhibitors) **(Figure 5E),** suggesting that FGF10 acts upstream of the effect of NOGGIN *ex vivo*. To further test this finding *in vivo*, we asked if the positive effect of FGF10 in regeneration-incompetent tadpoles could be abrogated by simultaneous NOGGIN addition. For this, we inserted beads co-loaded with FGF10 and NOGGIN to the amputation plane of regeneration-restricted/incompetent tadpoles and found this significantly decreased the positive effect of FGF10-only beads **(Figure 5G)**. These results further emphasise that FGF10 operates upstream of NOGGIN, and hence that secreted inhibitors play a dominant role in determining regeneration-outcome.

DISCUSSION

Limb regeneration and its requirement for a mature specialized wound epidermis (the AEC) is a well-established phenomenon with extensive tissue and gene level investigations. Here, moving beyond tissue-level descriptions, we reveal cell types and transcriptional states mediating *Xenopus* limb regeneration and AEC tissue by using single-cell transcriptomics and *ex vivo* regenerating limb cultures. Transcriptome and morphological assessment indicate that the transcriptional programmes and cells defining AEC and AER tissues are largely the same, differing only in the magnitude of their signaling center potential. Hence, AEC does not seem to involve a novel transcriptional programme specific for regeneration-competent species, but rather the activation of a programme that is highly reminiscent of developmental AER, at least in *Xenopus*. Moreover, by identifying transcriptomic and morphological differences between the specialized wound epidermis of an amputated tail and limb, we demonstrated that, at the cellular level, appendage-regeneration is context-dependent and warrants caution for cross-paradigm comparisons. Indeed, it is likely that other regeneration-paradigms may use different cell types and transcriptional programmes for their specialised wound epidermis (*e.g.* zebrafish fin AEC does not express *Fgf8* (Shibata et al., 2016)). Nonetheless, amniotes, including humans, have a developmental AER (Kelley and Fallon, 1976). Therefore, our results suggest that mammals have the transcriptional program to

orchestrate limb regeneration, but fail to redeploy the AER cell transcriptional program upon injury. These results prompted us to characterize regulators of AER cell formation.

Recent research has focused on the intrinsic properties of mesodermal tissue and its ability to induce specialized wound epidermis (via *Fgf10* expression), supported by the observation that transplantation of mesoderm tissue from regeneration-incompetent limbs prevents regeneration in -competent *Xenopus* limbs (Sessions and Bryant, 1988; Yokoyama et al., 2000). However, this approach is not able to discriminate whether cells are intrinsically incompetent or whether secreted factors cause this effect, as both would be transferred at the same time (as well as the numerous caveats associated with tissue transplantation). Moreover, this hypothesis does not explain why FGF10 is insufficient to induce AER cells across the entire epidermis, nor why regeneration outcomes are significantly correlated with the extent of ossification at the amputation plane (Dent, 1962; Nye and Cameron, 2005; Wolfe et al., 2000). Inspired by our scRNA-seq data, we sought to determine whether other secreted factors could also be contributing to regeneration incompetency. To our knowledge, there is no practical way to obtain secreted factors from -incompetent tadpoles and transfer them to -competent animals *in vivo*. Therefore, we established *ex vivo* cultures that faithfully recapitulated *in vivo* regeneration to test this critical hypothesis. We identified AER cells in the *ex vivo* limbs using spatially resolved and quantitative measurement of epidermal *Fgf8* via HCR (Choi et al., 2018). Our scRNA-seq data demonstrated that high epithelial *Fgf8* expression is a unique late-stage marker in the establishment of AER cell identity **(Figure 3D)**, and therefore *Fgf8* positivity in our experimental setup corresponds with high precision to the AER cell type. By using our explant systems and conducting co-culture and conditioned media experiments, both of which would be inaccessible *in vivo*, we found that secreted inhibitory factors in regeneration-incompetent tadpoles negatively impact AER cell formation.

To further explore this observation, we surveyed our scRNA-seq data and saw that a number of putative inhibitors (e.g. *Noggin*) were enriched in chondrogenic cell types, suggesting that factors secreted from the chondrogenic lineage may prevent AER cell formation. To test this hypothesis, we perturbed two genes previously associated with regeneration: *Noggin* (Beck et al., 2006; Pearl et al., 2008) and *Fgf10* (Yokoyama et al., 2001). Previous analysis of these genes was limited to the study of exogenous perturbations and their effect on regeneration outcome, without providing a model involving their endogenous function and their

interaction. For example, although Noggin overexpression was shown to block regeneration, we show here for the first time that secreted factors in regeneration-incompetent tadpoles block AER cell formation and that endogenous Noggin is one of the factors causing this effect. Similarly, although FGF10 was shown to restore regeneration competency, it was not known that FGF10 activity operates upstream of chondrogenesis and NOGGIN to influence regeneration-outcome. Altogether, in this work we have systematically assessed which cell types express *Fgf10* and *Noggin*, how they act on cell types to impact regeneration, and how they operate within our proposed cellular mechanism.

We then tested our model *in vivo* and found that indeed removal of secreted inhibitors (e.g. NOGGIN), or blocking the source of secreted inhibitors (chondrogenic progression via FGF10 application) could improve the regeneration-outcome in regeneration defective stages. Moreover, we demonstrated that NOGGIN attenuates the positive effect of FGF10 application, further highlighting the downstream role played by the secreted inhibitors. Overall, these results align with previous transplantation experiments showing that mesoderm from regeneration-incompetent limbs is inhibitory to regeneration (Sessions and Bryant, 1988; Yokoyama et al., 2001, 2000). However, in contrast to previous interpretations, we suggest that an important contributor to this phenomenon is the enrichment of chondrogenic cell abundance within the mesoderm tissue which express inhibitory secreted factors.

We further showed that by manipulating NOGGIN and FGF10 levels we could improve amputation-outcomes in regeneration-restricted/incompetent tadpoles. We see that anti-NOGGIN beads have a mild effect compared to FGF10 beads (**Figure 5A and 5G**), which may suggest that there are other inhibitors secreted from the chondrogenic lineage (e.g. *Chrdl1, Frzb*) that must also be eliminated to ensure robust regeneration. However, the mild effect of anti-NOGGIN may also be due to technical problems with the perturbation (e.g. limited duration and/or diffusivity of antibody delivery), and that a more complete inhibition of NOGGIN function would further improve the amputation-outcome.

It is well established that a salamander blastema will only form in a location distal to the amputation plane, a phenomenon termed as the rule of distal transformation (Butler, 1955; Nacu and Tanaka, 2011; Stocum, 1981). In our explants, we also detect that only distal sites started to form a blastema **(Figure 3A)**, aligning with the rule of distal transformation. Interestingly, by manipulating NOGGIN and FGF10, we also could observe AER cell

formation at the proximal sites of explants **(Figure 5F)**. However, it remains unclear if these proximal AER cells can enable the formation of a proximal blastema. Further work is required to investigate the relation between the rule of distal transformation and AER cells.

Benefiting from the stage-dependent regeneration-competency in *Xenopus*, our scRNA-seq datasets can discriminate true regeneration responses from injury responses. The majority of limb regeneration associated genes are derived from salamanders, where an injury control is not necessarily available (as these animals can always regenerate their limbs). We found that many genes associated with salamander limb regeneration (e.g. *Dpt, Prdx2*) (Gerber et al., 2018; Haas and Whited, 2017; Leigh et al., 2018) are upregulated upon injury in a subset of fibroblasts, regardless of regeneration competency. In a different context, recent single-cell analysis of mouse digit tip amputations suggests that, independent of the regeneration-outcome, some fibroblast populations express blastema-associated genes (e.g. *Prickle1, Fbn2, Lrrc17*) (Storer et al., 2020). We also see these genes upregulated upon injury in a subset of fibroblasts, but again this response is not specific to regeneration. These results suggest that there may be a conserved response to injury for mesenchymal cells in amphibians and mammals, and may be reflecting early suggestions by Tassava *et al.*, that an injury can induce morphologically assigned "dedifferentiation" that fails to establish a blastema without a specialized wound epidermis (Tassava and Loyd, 1977; Tassava and Mescher, 1975). Indeed, we observed lower levels of some regeneration-associated distal mesenchyme genes (e.g. *Shh*) in the subset of fibroblasts when there are no AER cells (**Figure S10**), correlating with regeneration-competency. Nonetheless, our results are insufficient to determine: (1) whether the fibroblast cells progressively become intrinsically incompetent to fully dedifferentiate or (2), without signals from signaling center potent AER cells, they fail to fully dedifferentiate. Moreover, although a subset of fibroblasts can express genes from multiple lineages, the functional consequences of this gain of transcriptional multipotency and how it resolves during varying stages of regeneration-competency remain unclear. Further work on injury-induced mesenchymal plasticity, its interaction with AER cells, and cross-species comparison on this topic will be required. Nevertheless, these results underscore that caution is needed when interpreting experiments involving injury (e.g. transplantation), as well as the concern that previously implied "regeneration-genes" may be injury response genes.

Overall, we propose a new cellular model of regeneration incompetency, in which chondrogenesis associated secreted factors inhibit AER cell formation. Although it remains unclear if chondrogenesis itself directly inhibits limb regeneration, there are multiple observations from our work and others that support this hypothesis (Dent, 1962; Nye and Cameron, 2005; Wolfe et al., 2000). Our model suggests new avenues for cross-species studies aiming to decipher limb development and regeneration, and can explain why *Xenopus* limb amputations at proximal versus distal sites exhibit different regeneration outcomes, since proximal sites are associated with more advanced stages of chondrogenesis (Dent, 1962; Nye and Cameron, 2005; Wolfe et al., 2000). Furthermore, the pace of chondrogenesis may have an association with limb regeneration ability across species, such that terrestrial warm-blooded animals may have a more robust and fast-paced chondrogenesis program compared to regeneration-competent aquatic cold blooded animals. Indeed, limb regeneration-incompetent species such as chicken or mouse have a faster limb chondrogenesis program during their development compared to regeneration-competent axolotl and *Xenopus*. Additionally, although a side-by-side comparative study would be required, mice bone fractures were documented to heal faster compared to axolotl bone fractures (Hutchison et al., 2007; Vortkamp et al., 1998). It is well-established that chondrogenic programs are heavily influenced by BMP pathway activity. The ratio of BMP agonist/antagonist (*e.g.* BMP4/NOGGIN) during development, injury, or upon limb amputation may be different between limb regeneration-competent and -incompetent animals. This difference may also be connected to observed *Noggin* phenotypes across species. Specifically, adding exogenous *Noggin* results in extended AER maintenance in chicken (Pizette & Niswander, 1999) and mouse (Wang et al., 2004), whilst it abolishes AER in *Xenopus* (Jones et al., 2013). Targeted comparative studies on these topics will be subject of future work.

It remains unclear how our identified cellular mechanisms are associated with robust regenerative abilities of some salamanders. Based on current results, regeneration-competent axolotls are suggested to not have a developmental AER (Purushothaman et al., 2019), but can form AEC. Meanwhile AER associated FGFs are expressed in axolotl mesenchyme (Purushothaman et al., 2019). Hence, it is tempting to speculate that limb regeneration-competent salamanders could withstand inhibitory secreted factors because of the location and, potentially, higher absolute amount of AER cell signals in mesenchymal rather than epidermal cells. Additionally, in contrast to axolotl limb regeneration, where a more

homogenous mesenchymal transcriptional response was suggested (Gerber et al., 2018), we identified only a subset of fibroblast populations can gain transcriptional multipotency and express genes associated with blastema. Whether these differences between species result in more robust regenerative abilities requires further work.

Finally, in this work we have identified a cellular mechanism governing regeneration-incompetency in in developing tadpoles, although it remains unclear whether similar principles apply in adult frogs with a more definite limb. Manipulation of chondrogenic programs in adult frogs and other regeneration–incompetent species may lead to novel approaches to promote limb regeneration, albeit with additional barriers to regeneration (*e.g.* scarring and more complex immune responses) that may have to be overcome. Altogether, our work suggests a new cellular model of limb regeneration **(Figure 6)**, which unites disparate tissue and gene level findings in the field, and suggests that modulation of secreted factors impacting on epidermal populations has the potential to unlock the ability to regrow lost limbs in non-regenerative higher vertebrates.

MATERIALS AND METHODS

Tadpole generation and husbandry.

Tadpoles were generated and staged as previously described (Aztekin et al., 2019). After NF Stage 45, tadpoles were fed once or twice a day with filamentous blue-green algae (ZM spirulina powder) suspended in water. Wild-type *Xenopus laevis* were used for experiments unless otherwise stated. Tadpoles classified as regeneration-competent were NF Stage 52-53, regeneration-restricted were NF 55-56, and regeneration-incompetent were NF Stage 58-60. Animal experiments were approved by the University Biomedical Services at the University of Cambridge and complied with UK Home Office guidelines (Animal Act 1986).

Single-cell dissociation, library preparation and sequencing.

For developmental samples, tadpoles were killed, and samples were collected at the aforementioned stages. For amputation/regeneration samples, tadpoles were anaesthetized by incubating them with 0.1X MMR 0.002% MS222 (A0377876, Acros Organics), placed on a wet towel and the right hindlimbs were amputated at the presumptive knee/ankle level for regeneration-competent tadpoles, and at the ankle level for –restricted or –incompetent tadpoles. Afterwards, the tadpoles were returned to fresh water. At 5 days post amputation

(dpa), tadpoles were killed and the newly generated tissues on the amputation plane were collected. Contralateral control samples were also collected from these tadpoles, and intact limb buds or autopods including ankle were collected. For each scRNA-Seq experiment, tissues were collected from a total of 8-10 tadpoles to reduce variance caused by staging differences. Dissociations were performed on a pool of 4 limbs in an Eppendorf tube with the following protocol. First the samples were washed with Ca-Mg free 1X MBS ((Barth-HEPES Saline) 10X stock: 88 mM NaCl, 1 mM KCl, 2,4 mM NaHCO3, 0.82mM MgSO4.7H2O, 0.33mM Ca(NO3)2.4H2O, 0.41 mM Cacl2.6H2O, 10 mM HEPES. Add ~3 mL of 10N NaOH to obtain a pH of 7.4 to 7.6). Samples were then incubated with 1X Trypsin (Sigma, 59427C) in Ca-Mg free 1X MBS with 0.5 μM EDTA for 10 minutes at room-temperature (RT) on a bench-top shaker at a speed of 300 rpm. Trypsin reaction was diluted with Ca-Mg free 1X MBS after 10 minutes. Physical dispersion was applied (10-15 times up-down trituration with a pipette) to samples before, half way, and at the end of trypsinisation. Cells were spun down at 250 g for 5 minutes, the supernatant was taken out, and cells were then resuspended in 1X Ca-Mg free 1X MBS. Cells were passed through a 35 μm diameter cell strainer then stained with 20 μM Hoechst 33342 (Sigma, 2261) in 1X Ca-Mg free MBS for 10-15 minutes, and Hoechst positive cells were sorted using a Sony SH800s Cell Sorter. scRNA-seq libraries were generated using 10X Genomics (v3 chemistry) and sequenced in pools of 2 samples per lane on an Illumina Novaseq 6000 SP flow cell, with the following parameters: 28 bp - read 1; 8 bp - i7 index; and 91 bp - read 2, as per standard 10X Genomics recommendations.

scRNA-seq: data processing.

Output files from 10X Genomics were processed using CellRanger v3.0.2, with sequences mapped to the *Xenopus* laevis 9.1 genome (Xenbase, ftp://ftp.xenbase.org/pub/Genomics/JGI/Xenla9.1/Xla.v91.repeatMasked.fa.gz and ftp://ftp.xenbase.org/pub/Genomics/JGI/Xenla9.1/1.8.3.2/XL_9.1_v1.8.3.2.allTranscripts.gff3.gz). Raw counts were normalized by cell library size, and then converted to TPX (transcripts per 10^4). Cell calling was performed using CellRanger with default parameters. We further filtered the data according to library size, discarding cells with a total UMI count in the lowest quartile. We note that the main cell types and transcriptional changes remained unchanged if we omitted this cell-filtering step, although the clustering and visualization appears less robust (Figure S4).

scRNA-seq: feature selection.

Highly variable genes (HVGs) were selected for clustering and visualization as described previously (Aztekin et al., 2019) (Fano factor > 65^{th} percentile, mean expression > 5^{th} percentile and mean expression < 80^{th} percentile). Our initial analysis revealed that visualization and clustering was strongly influenced by cell cycle state (Figure S2). To further refine the set of HVGs, we performed factor analysis with the aim of removing genes significantly associated with the cell cycle. Specifically, non-negative matrix factorization was performed on the cosine normalized, log2-transformed normalized counts matrix, using k = 30 components (R package *nnlm*). Factors were manually annotated according to their expression on the UMAP projection, and by inspection of the highest gene loadings for each factor; 2 factors corresponded to the cell cycle. To minimize the effect of the cell cycle signature on projection/clustering, we identified genes associated with these cell cycle factors (top 10% gene loadings for each factor) and removed these from the set of HVGs.

scRNA-seq: visualization and clustering.

Data were projected onto two dimensions using the UMAP algorithm (Becht et al., 2019), with log2-transformed HVGs, cosine distance as a similarity measure, and parameters k = 15, min_dist = 0.2. Clustering was performed as described previously (Aztekin et al., 2019). Briefly, we constructed a graph using the UMAP function *fuzzy_simplicial_set* with k = 10 nearest-neighbors, and then performed graphical clustering using the walktrap algorithm (*cluster_walktrap* from R package *igraph*, with steps = 10).

scRNA-seq: gene set enrichment and cell cycle analysis.

Single cell gene set enrichment scores were calculated with the *AUCell* R package (Aibar et al., 2017), using HVGs as the background gene set. Cell cycle phase was inferred using *CellCycleScoring* (R package *Seurat*) (Butler et al., 2018).

scRNA-seq: annotation of cell-types.

Cell type annotation was performed by manually comparing cluster-specific gene expression patterns (computed using *findMarkers* in R package *scran* (Lun et al., 2016)) with known cell type markers from the literature. Many clusters could be assigned to a well-characterized, functional cell type (e.g. *Satellite cell*). Other clusters could not be unambiguously identified, but were assigned a broad label together with a numeric identifier (e.g. *Blood 1*). Finally, a

few clusters remain unannotated (e.g. *Unknown 1*). Dotplots of key marker genes of each cell type are provided in Figure S5.

scRNA-seq: gene expression visualization.

Gene expression in individual cells is visualized on the UMAP projection with points colored according to expression level (log10-transformed). Gene expression across groups of cells (e.g. for different clusters, or for different stage tadpoles) is shown using dotplots colored by mean expression (log10-transformed, normalized to group with maximal expression). We can detect alleles from both the Large (*Gene.L*) or Short (*Gene.S*) chromosomes present in the pseudotetraploid *Xenopus laevis* genome. In some figures, we report expression from both the large and short allele; in others, we report whichever allele has higher expression for brevity. Differentially expressed genes were identified using the *findMarkers* function (using default parameters, and comparing cells from different conditions); results were then visualized as volcano plots.

Regeneration assay and bead experiments.

Affi-gel blue gel beads (Bio-rad, **1537301**) were incubated with the following proteins overnight at 4 degrees: 2-3 μg Rabbit-IGG isotype control antibody (ab37415); 2-3 μg anti-NOGGIN antibody (ab16054); 0.1% BSA; 1 μg recombinant human FGF10 (R&D, 345-FG) in 1-2 μl 0.1% BSA; 1-1.5 μg recombinant human FGF10 (R&D, 345-FG) and 2.5-4 μg recombinant human NOGGIN (R&D, 6057-NG) in 3-4 μl 0.1% BSA. Tadpoles were anaesthetized with 0.002% MS222, placed on a wet towel, and both right and left hindlimbs were amputated from ankle level in either –restricted or –incompetent tadpoles. 3-4 beads were placed on the amputation plane of the right hindlimb. Left hindlimbs served as an internal control for the experiments. Please note that pushing the bead deep in the tissues at the amputation site was avoided as much as possible, and beads were gently positioned instead. Tadpoles were monitored on a wet towel for 3-5 minutes then tadpoles that kept the beads were placed in fresh water. Tadpoles were killed in between 18-21 dpa to assess the regeneration outcome. The difference in the number of digits or digit-like structures between the right to the left limb was quantified for each tadpole.

Whole-mount mRNA visualization, hybridization chain reaction (HCR), with or without combination of immunofluorescence or histology

<u>HCR on whole limb or tail samples</u>

HCR was applied as described before (Choi et al., 2018) with modifications, and materials for HCR were purchased from Molecular Instruments Inc unless otherwise stated. Limb and tail samples were fixed with 4% formaldehyde in 1X PBS for 40-60 minutes, permeabilized in 70% ethanol in 1X PBS for 2-4 hours, washed briefly with 1X PBS and collected in Eppendorf tubes. These procedures were carried out on a rotator at RT. The supernatant was taken out, 500 µl wash solution (Molecular Instruments Inc.) was added, and samples were rotated at RT for 5 minutes. The supernatant was taken out and replaced by 400-500 µl hybridization buffer (Molecular Instruments Inc.) for a 30 minutes incubation at 37 degrees. In parallel, the probe solution was prepared by diluting mRNAs targeting probes to 30-40 nM in 200 µl hybridization buffer and incubated for 30 min at 37 degrees. The hybridization buffer from samples were taken out and probe solution was placed on samples for a 12-16 hours incubation at 37 degrees. Subsequently, the samples were washed 2 x 20 minutes with wash buffer, and 2x30 minutes with 5x SSC-T at RT. To visualize probes, amplification solution was prepared by first heating to 95 degrees for 90 seconds the fluorophore attached hairpins pairs (h1 and h2 hairpins) that matches to the probes. Hairpins were then left in dark at RT for 30 minutes. Afterwards, final amplification solution was prepared at 40-60 nM h1 and h2 in 200 µl amplification buffer. Afterwards, samples were first incubated in amplification buffer without hairpins for 10 minutes, then placed in final amplification solution at room temperature, protected from light, for 12-16 hours on a rotator. Samples were washed with 2x20 min SSC-T. Samples were then put in 1X PBS.

Whole-mount HCR samples imaging: For stereomicroscope or confocal imaging of whole samples, the samples were mounted in 0.6%-0.8% ultra-low gelling temperature agar (Sigma, A5030) in 1X PBS.

Sectioning of samples after HCR:

In the subsequent step of the protocol, the samples were protected from light to preserve the HCR signal. The samples were incubated in 15% sucrose in 1X PBS at RT for 1 hour, then 30% sucrose in 1X PBS at 4 degrees overnight. Samples were then placed in O.C.T. solution and incubated at -80 overnight. Samples were cryosectioned to 5 µm thickness, stained with 20 µM Hoechst (Sigma, 2261) in 1X PBS at RT for 10 minutes and imaged.

Immunostaining

After sectioning of HCR stained limb, the samples were processed for immunostaining.

Samples were blocked with 50% Cas-Block (Invitrogen, 008120) in 1X PBS-T (1X PBS + 0.1 Tween-100) and incubated for 30 minutes in room temperature without rotating. Samples were then incubated with antibodies (listed below) at 4 degrees overnight without rotating. Samples were washed with PBS-T for 2x10 minutes, blocked by 50% Cas-Block in 1X PBS-T for 30 minutes, and incubated with secondary antibodies (listed below) for 1 hour, all these steps were carried out at RT without rotating. Samples were washed with 1X PBS-T for 2x10 minutes and 2x20 minutes 1X PBS at RT without rotating. After antibody staining, samples were stained with Hoechst and washed with 1x5 min 1X PBS at RT without rotating. Samples were mounted in 80% Glycerol in 1X PBS with a coverslip and imaged.

Tail whole-mount HCR staining can be combined with whole-mount immunofluorescence by following the above immunofluorescence protocol except that the mounting of whole-tails were done in ultra- low gelling temperature agar for imaging.

HCR probes and Hairpins: Probes for *Fgf8.L*, *Dpt.L*, *Htra3.L*, *Prrx1.L* and *Sp9.L* were purchased from Molecular Instruments Inc.. Probes were designed against the full-length *Xenopus Lgr5.S*, *Msx1.L*, and *Fgf10.L* mRNA sequence as described by (Choi et al., 2014). HCR Hairpins were purchased from Molecular Instruments Inc.

Primary antibodies, and working dilutions: TP63 [4A4] (Abcam, ab735, 1:200), B-CATENIN (Abcam, ab6302, 1:2000), E-CADHERIN (5D3, DSHB, 1:10), ITGB1 (8C8, DSHB, 1:10), anti-EGFP (Abcam, ab13970, 1:500).

Secondary antibodies: goat anti-chicken IgY (H+L) secondary antibody, Alexa Fluor 488 (Invitrogen, A11039, 1:500), goat anti-mouse IgG (H+L) cross-adsorbed ReadyProbes secondary antibody, Alexa Fluor 594 (Invitrogen, R37121, 1:500). goat anti-mouse IgG (H+L) cross-adsorbed ReadyProbes secondary antibody, Alexa Fluor 488 (Invitrogen, R37120, 1:500).

Leica SP8 upright confocal microscope with a 40x/1.3 HC PL Apo CS2 Oil objective was used for all confocal images except for Figure S9B&C images which were taken with Leica SP8 inverted confocal microscope with a 20x/0.75 HC PL Apo CS2 Multi. LAS X was used for setting tiled images, and 20% overlap between tiles were used. Limb whole-mount HCR images were taken via a Leica stereomicroscope equipped with a DFC7000 T camera. Fiji

was used for maximum projection of z-stacks and to adjust contrast to highlight biological relevance. If needed, images were cropped, flipped, and/or rotated to highlight biological relevance.

Histological staining can be done on top of cryosectioned HCR samples. Briefly, samples were stained with hematoxylin and eosin according to manufacturer`s protocol (Abcam, ab245880), afterwards samples were stained for Alcian Blue (Sigma, B8438**)** according to manufacturer`s protocol**.** Histology images were taken on a Zeiss AxioImager compound microscope.

***Ex vivo* limb culture method to assess AER cell formation and proximal chondrogenesis**

Limbs were first amputated from presumptive knee/ankle level for – competent and ankle level for –restricted or –incompetent tadpoles. The distal parts of these amputated explants were then removed and the remaining proximal segment was placed in 1000, 500, 200 µl explant media (L-15 (Thermo, 11415064) 1X Antibiotic-Antimycotic (Thermo, 15240062), 20% Fetal Bovine Serum Superior (Sigma, S0615)) in 12, 24, or 96-well plates, respectively. Explants were cultured for 3 days without changing the media. After 3 days, to quantify AER cell formation the explants were fixed and proceeded to HCR protocol; to quantify proximal chondrogenesis the explants were fixed with 4% formaldehyde, mounted in 0.6% Low-Melt agar, and directly imaged via Stereomicroscopy. Explants emit autofluorescence. Though the abundant HCR signal can be seen despite the autofluorescence, to discriminate the HCR signal from autofluorescence in finer detail, sample images were taken in red and green channel separately with the same exposure and gain settings, and then merged in Fiji. In merged images, the background signal due to autofluorescence was visualized as yellow and the HCR signal was either red or green. As AER cells were largely detected as a monolayer population, AER cell formation was calculated by measuring the length of the *Fgf8.L* signal on the amputation plane using Fiji segmented line option. The proximal chondrogenesis can be visually distinguished, and to determine the chondrogenesis length, chondrogenic structure length from top to bottom was also measured using Fiji. Samples where a clear chondrogenesis was not visible were omitted from further analysis. These images were taken in brightfield imaging and measurements were done in Fiji.

For drug and recombinant protein treatments, the explants were placed in culture media containing the following small molecules concentration or recombinant protein amounts,

unless otherwise stated: 100 μM ICRT3 (Sigma, SML0211), 100 μM SU-5402 (Sigma, SML0443), 50 μM SB-505124 (Sigma, S4696), 100 μM DAPT (Sigma, D5942), 2.5 μM LDN-193189 (Stemgent, 04-0074), 500 ng human recombinant FGF10 (R&D, 345-FG), 1.25 μg human recombinant NOGGIN (R&D 6057-NG), and 500 ng human recombinant BMP4 (R&D, 314-BP). Drugs were prepared in DMSO, and recombinant proteins were prepared in 0.1% BSA. Small molecule experiments were conducted in 24-well plate. Recombinant protein experiments were done in 96-well plate. Max 5-6 explants were placed in 24-well plates. 1 explant was put in one well of 96-well plate for recombinant protein treatments. In all chemical and recombinant protein perturbation experiments, one limb of the same animal was subjected to the perturbation, and the contralateral limb served as a control. These control explants were exposed to solution containing matching DMSO or BSA concentration in 1X PBS for chemical or recombinant protein perturbations, respectively. Perturbation and control samples were pooled separately at the end of experiments and proceeded with staining.

EdU Labelling.

Ex vivo limbs were cultured with 10 μM EdU (Thermo, C10337) for 3 days in dark foiled cover. Afterwards, samples were fixed, and *Fgf8.L* mRNA was stained using the HCR protocol, followed by cryosectionning, as described above. Sections were subjected to Click-It reaction as described in manufacturer`s protocol (Thermo, C10337). Hoechst was added at the end of the protocol. Samples were visualized by confocal microscopy as described above. (1) *Fgf8.L* positive cells, and (2) EdU positive and *Fgf8.L* positive cells on the amputation plane were manually counted, and the percentage of EdU positive *Fgf8.L* positive cells were calculated for each sample.

Bead experiment for proximal chondrogenesis.

Beads were prepared as described above. Explants from –restricted tadpoles were harvested as described above and beads were implanted on the proximal site of explants. At 3 dpa, explants that did not contain bead at their proximal site anymore (presumably due to repelling) were omitted from further analysis. At 3 dpa, samples were imaged without fixation and the extent of chondrogenesis was measured by Fiji.

DiO Labelling.

DiO (DiO'; $DiOC_{18}(3)$ (3,3'Dioctadecyloxacarbocyanine Perchlorate), Thermo, D275) was prepared by dipping a tip in the DiO containing powder tube, and placing the tip in a 10 µl 100% ethanol containing Eppendorf. A glass needle tip was then dipped in the diluted DiO solution and harvested *ex vivo* limbs were labelled on a wet towel. These cultures were placed in *ex vivo* culture media and explants were imaged every day with a stereomicroscope.

***Ex vivo* limb co-culture, and conditioned media experiments**.

For co-culture experiments, one -competent and one –incompetent limb explants were incubated together in 200 µl explant media in a well of 96-well plate. For antibody experiments, one limb of each animal served as a control and was incubated with 1 µg Rabbit-IGG isotype control antibody (ab37415) while the contralateral limb was incubated with 1 µg anti-NOGGIN antibody (ab16054). Antibodies and media were only added at the beginning of the cultures and were not replaced during the experiment.

For conditioned media experiments, conditioned media supplying and receiving explants were prepared separately. Supplying explants were prepared one day before harvesting receiving explants and incubated in 200 µl explant media in a well of 96-well plate. After one day, media from the supplying explant was collected and used to culture the newly harvested receiving explant, and a fresh media was added for supplying explant. This change of media procedure was repeated for 3 days. For antibody experiments, supplying explant media was collected and pre-incubated with 1 µg antibodies for 25-30 minutes at RT on a rotator, then the pre-incubated media was placed on the receiving explants.

Replicate information and statistical tests.

Sample sizes were not pre-determined in any experimental setup. In this work, biological replicates refer to samples obtained from multiple animal batches and to experiments carried out on different days. In all experiments, the number of independent tadpole limbs assayed is recorded and denoted by *n* in the text and figure legends. In all experiments, wild-type tadpoles were used from tanks that contain multiple batches (tadpoles raised from different father and/or mother). In all explant perturbation experiments, samples were compared to their contralateral controls, and a Mann Whitney U test was used to determine statistical significance. For regeneration and bead experiments, a t-test was used. To assess the significance of proximal *Fgf8* expression in explants (Figure 5f), Fisher's exact test was used.

Data and code availability.

Code is available at https://github.com/MarioniLab/XenopusLimbRegeneration2020. Sequencing data, together with processed counts matrices, are available on ArrayExpress with the accession number E-MTAB-9104. We provide an interactive online tool to explore our dataset https://marionilab.cruk.cam.ac.uk/XenopusLimbRegeneration/

ACKNOWLEDGEMENTS

We thank Katarzyna Kania and the Cambridge Institute Genomics Core for their support with this work on the 10X-Genomics and sequencing library preparations. The transgenic testes used in this study was obtained from the European Xenopus Resource Centre, curated with funding from the Wellcome Trust/BBSRC, and maintained by the University of Portsmouth, School of Biological Sciences. We thank R. Jones-Green for excellent animal care. We thank H. Ma for use of her stereomicroscope, and E. Rawlins for use of her Zeiss Axiolmager compound microscope. We thank B. Steventon, E. Rawlins, and members of the Marioni and Simons labs for general discussion about the project. We thank R. Butler for assistance in image analysis.

COMPETING INTERESTS

The authors declare no competing interests.

AUTHOR CONTRIBUTIONS

Conceptualization: C.A. with contributions from other authors; Methodology: C.A., and T.W.H. for computational analysis; Software: T.W.H.; Validation: C.A., T.W.H.; Formal analysis: T.W.H. with help from C.A.; Investigation: C.A.; Resources: J.B.G., J.C.M.; Data curation: C.A., T.W.H; Writing – original draft: C.A. with help from J.J.; Writing - review and editing: C.A., T.W.H, J.J., B.D.S., J.C.M.; Supervision: J.B.G., J.C.M., J.J., B.D.S.; Project administration: C.A.; Funding acquisition: C.A., J.J., J.B.G., B.D.S., J.C.M.

FUNDING

C.A. is funded by University of Cambridge and Cambridge Trust. J.J. and J.B.G. are funded

by a grant from the Wellcome Trust (101050/Z/13/Z). T.W.H., J.C.M., and B.D.S. are funded as part of a Wellcome Strategic Award to study cell fate decisions (105031/D/14/Z). T.W.H. is also supported by an EMBO Long-Term Fellowship (ALTF 606-2018). B.D.S. also acknowledges funding from the Royal Society E.P. Abraham Research Professorship (RP\R1\180165) and Wellcome Trust (098357/Z/12/Z). J.C.M. acknowledges core funding from the European Molecular Biology Laboratory and Cancer Research UK (A17197). This work is funded by a grant from the Wellcome Trust (101050/Z/13/Z), Molecular Research Council (MR/P000479/1), and supported by the Gurdon Institute core grant from Cancer Research UK (C6946/A14492) and the Wellcome Trust (092096/Z/10/Z).

Figure 1. Single-cell transcriptomics reveals cellular heterogeneity in developing and amputated *Xenopus* limbs at different stages of regeneration competence.

a, Schematic describing *Xenopus* limb regeneration at different NF Stages. NF Stage ~52-54 tadpoles are regeneration-competent and amputations result in regeneration of a full limb. Regeneration-ability begins to decline at NF Stage ~54. Tadpoles are regeneration-restricted at NF ~Stage 56, where 2-3 digits can be regenerated. Beyond NF Stage ~58, tadpoles are regeneration-incompetent and amputations result in simple wound healing or unpatterned spike formation. Green boxes indicate the samples collected for scRNA-seq, taken at stages prior to, at the onset of, and after the loss of regeneration ability. **b**, Schematic describing 5 days post amputation (dpa) samples for regeneration-competent, -restricted, and –incompetent tadpoles. Green boxes show the samples collected for scRNA-seq. **c**, An atlas of cell types in intact and amputated limbs. Samples from each condition are processed separately for sequencing, and are then pooled together for UMAP visualization and clustering. Each dot corresponds to a single cell, colors indicate cluster identity, text labels important tissue/cell types. See Figure S3 for full annotation. **d**, Comparisons can be made between conditions to highlight transcriptional changes associated with regeneration; here NF Stage 52 amputated limbs (lower) are compared to their contralateral control samples (upper). Red dots denote cells in the selected sample; grey dots denote cells in all samples. **e**, Diversity of mesenchymal cell types detected in our dataset (upper), together with putative gene expression programs identified using unbiased factor analysis (lower).

Figure 2. Formation of a signalling centre comprising apical-ectodermal-ridge (AER) cells is associated with the successful regeneration.

a, Multiple basal epidermal cell states are detected, including AER cells, in the pooled dataset. **b**, UMAP visualization of basal epidermis reveals that re-establishment of AER cells is associated with successful regeneration. Red dots denote cells in the selected sample; grey dots denote cells in all samples. **c**, (Left) UMAP visualization of pooled data for AER cells expressing *Fgf8.L*. (Right) Stereomicroscope images of the 5 dpa amputation plane of regeneration-competent, -restricted, and –incompetent tadpoles. *Fgf8.L* (red) expressing AER cells are formed in regeneration-competent and –restricted tadpoles, but not in regeneration–incompetent tadpoles. Scale bar = 250 μm. **d**, Abundance of basal epidermal cell types across conditions reveals a correlation between AER abundance and regeneration outcome. AER cells are present in intact regeneration–competent samples, and are enriched after amputation. A similar pattern is seen in regeneration-restricted samples, although abundances of AER cells are reduced. Very few AER cells are detected in regeneration–incompetent tadpoles. **e**, Dot plot showing expression of selected ligands for AER cells during development and at 5 dpa in regeneration-competent, and -restricted samples. Dot color indicates mean expression; dot size represents the percentage of cells with non-zero expression.

Figure 3. *Ex vivo* regenerating limbs demonstrate that AER cell formation requires activation of multiple pathways and can form from basal epidermal cells.

a, (Left) Schematic for *ex vivo* regeneration limb culture. (Right) Time-lapse images of a regeneration–competent explant. The explant grows a cone shape at its distal site reminiscent of *in vivo* regeneration (green arrow), whilst the proximal site shows chondrogenesis (blue arrow). Scale= 200 μm. **b**, Example image of a regeneration–competent explant at 3 days post-culture. Distal site of explants is *Fgf8.L* positive (red arrow), and proximal site is *Fgf8.L* negative (purple arrow). Red, *Fgf8.L* mRNA. Scale= 200 μm. **c**, Drug screen to test regulators of AER cell formation. (Top) Schematics describing the screen. One limb of a tadpole was used for perturbation and the contralateral limb from the same tadpole was used as a control. Samples were treated with the indicated drugs for 3 days post-culture, and then stained for *Fgf8.L* mRNA. The extent of *Fgf8.L* expression along the amputation plane was measured. Sample sizes: ICRT3 total n≥9 from 3 biological replicates; SU5402 total n≥9 from 2 biological replicates; LDN193189 total n=8 from 3 biological replicates; SB431542 total n= 8 from 2 biological replicates; DAPT total n=7 from 3 biological replicates. *P**<

0.05, and *P***< 0.001. **d**, Factor analysis identifies a putative gene expression trajectory from basal epidermal cells to AER cells, predicting sequential activation of *Lgr5.S* followed by *Fgf8.L*. **e**, A proximal-to-distal gradient of *Lgr5*.S and *Fgf8.L* is observed in *vivo*, with *Fgf8.L* being restricted to the most distal regions of the midline epidermis. Black dots represent HCR mRNA signal. Scale = 20 μm.

Figure 4. Inhibitory factors, such as Noggin, are secreted from chondrogenic populations at regeneration incompetent stages, and block AER cell formation.

a, (Top) Schematic describing co-culture experiments. (Mid) Co-culturing (CC) regeneration-competent and –incompetent explants decrease the extent of *Fgf8*.L expression at the amputation plane at 3 dpa. (Bottom) This effect can be rescued by adding anti-NOGGIN antibody. Regeneration-competent and –competent CC: total n=26, from 4 biological replicates; regeneration-competent and –incompetent CC: total=15, from 4 biological replicates; competent and –incompetent CC and anti-IGG antibody: total n=10, from 3 biological replicates; competent and –incompetent CC and anti-NOGGIN antibody: total n=10, from 3 biological replicates. *P**< 0.05, and *P***< 0.001. **b**, (Top) Schematic describing conditioned media experiments to test the effect of secreted factors in regeneration-incompetent tadpole limbs. (Mid) Supplying conditioned media (CM) from regeneration-incompetent tadpoles to regeneration-competent explants decreases the extent of *Fgf8*.L expression at the amputation plane at 3 dpa. (Bottom) This effect can be rescued by adding anti-NOGGIN antibody. Regeneration-competent CM to –competent explants: total n=8, from 3 biological replicates; regeneration-incompetent CM to –competent explants: total n=7, from 3 biological replicates; regeneration-incompetent CM to –competent explants and anti-IGG antibody: total n=10, from 3 biological replicates; -incompetent CM and anti-NOGGIN antibody to –competent explants: total n=10, from 3 biological replicates. *P**< 0.05, and *P***< 0.001. **c**, Abundance of mesenchymal populations across conditions reveals an enrichment of chondrogenic populations at regeneration-restricted and -incompetent stages, in both intact and amputated limbs. **d**, Multiple BMP/WNT antagonists are expressed specifically in chondrogenic populations. Note that this dotplot is generated using the pooled dataset, with late-stages tadpoles having an enrichment in chondrogenic and fibroblast populations but not immature mesenchymal cell types, as shown in Figure 4c.

Figure 5. FGF10 impacts chondrogenesis and operates upstream of NOGGIN.

a, Anti-NOGGIN antibody application to distal amputations improve regeneration in –restricted and –incompetent tadpoles. –Restricted and –incompetent tadpole right and left hindlimbs were amputated and beads containing anti-IGG antibody or anti-NOGGIN antibody were placed on the right hindlimbs. Formed digits and digit-like structures were quantified in the right and left hindlimbs and the difference calculated. Anti-IGG antibody total n=17 from 3 biological replicates; Anti-NOGGIN antibody total n=28 from 4 biological replicates. **b**, The effect of FGF10 on chondrogenesis is assessed by measuring the chondrogenic outgrowth at the proximal sites of -restricted explants at 3 dpa. Implanting 0.1% BSA/PBS beads to the proximal site or supplying 0.1% BSA/PBS to the media had no significant effect on chondrogenesis while implanting Fgf10 beads to the proximal site or supplying FGF10 in media reduced chondrogenesis. Contralateral limbs were used as control and labelled as empty. From left to right, empty and PBS beads total n ≥7, from at least 2 biological replicates; empty and FGF10 bead total n ≥ 14, from at least 4 biological replicates; empty and 0.1% BSA/PBS in media total n=10 from 3 biological replicates; empty and FGF10 in media ≥ n=14 from at least 3 biological replicates. ns = not significant, *P**< 0.05, and *P***< 0.001. **c**, (Left) Example images of SU5402 treated explant showing extensive chondrogenesis at the proximal site. (Right) Blocking FGFR via small molecule inhibitor SU5402 extends chondrogenesis in 3 days for –competent and –restricted explants. Contralateral limbs were used as control and treated with DMSO. DMSO total n= 29, from 7 biological replicates, and SU5402 total n=25 from 7 biological replicates. *P***< 0.001. **d**, Example sectioned histology images for 3 dpa explants treated with SU5402. The outgrowing structure are alcian blue rich indicative of chondrogenic cells. **e**, Regeneration-competent explants were treated with combination of FGF10 and recombinant BMP4, or recombinant NOGGIN, or LDN193189, or anti-NOGGIN antibody. 0.1% BSA/PBS and anti-IGG antibody were used as controls. From left to right, BSA: total n=8 from 2 biological replicates; recombinant FGF10 and recombinant BMP4: total n=8 from 2 biological replicates; DMSO and BSA: total n=8 from 2 biological replicates; FGF10 and LDN total n=8 from 2 biological replicates; BSA and anti-IGG antibody: total n= 12 from 3 biological replicates; FGF10 and anti-NOGGIN antibody: total n=10 from 3 biological replicates; BSA: total n=8 from 2 biological replicates; recombinant FGF10 and recombinant NOGGIN: total n= 8 from 2 biological replicates. *P**< 0.05, and *P***< 0.001. **f**, Example whole-mount stereomicroscope image of rFGF10 and anti-NOGGIN antibody treated explants can show a substantial *Fgf8.L* expression at different sites of the explant (n=5/9 from 2 biological replicates, compared to n=0/121 in controls, $P < 0.0001$). Scale, 200 μm. **g,** Recombinant

FGF10 application to distal amputations restore regeneration in –restricted and –incompetent tadpoles. –Restricted and –incompetent tadpole right and left hindlimbs were amputated and beads containing 0.1% BSA/PBS or recombinant FGF10 or recombinant FGF10 and NOGGIN were placed on the right hindlimbs. Formed digits and digit-like structures were quantified in the right and left hindlimbs and the difference calculated. Empty total n=19 from 2 biological replicates; 0.1%/PBS bead total n=17 from 5 biological replicates; recombinant FGF10 bead total n=25 from 5 biological replicates; recombinant FGF10 and NOGGIN bead total n=25 from 4 biological replicates. ns = not significant, *P***< 0.001.

Figure 6. Secreted inhibitory factors associated with chondrogenic progression block AER cell formation.

Secreted factors such as WNTs and BMPs support AER cell formation at the amputation plane. During development, chondrogenesis leads to the accumulation of secreted inhibitory factors including NOGGIN, which results in failure to establish AER cells (*Fgf8.L+/Lgr5.S+).* FGF10 can suppress chondrogenesis. Amputations, independent of the regeneration outcome, induce injury-induced mesenchymal transcriptional plasticity.

REFERENCES

Lun ATL, McCarthy DJ and Marioni JC. A step-by-step workflow for low-level analysis of single-cell RNA-seq data with Bioconductor [version 2; peer review: 3 approved, 2 approved with reservations]. *F1000Research* 2016, **5**:2122 https://doi.org/10.12688/f1000research.9501.2Aibar, S., González-Blas, C.B., Moerman, T., Huynh-Thu, V.A., Imrichova, H., Hulselmans, G., Rambow, F., Marine, J.-C., Geurts, P., Aerts, J., van den Oord, J., Atak, Z.K., Wouters, J., Aerts, S., 2017. SCENIC: single-cell regulatory network inference and clustering. Nature Methods 14, 1083–1086. https://doi.org/10.1038/nmeth.4463

Aztekin, C., Hiscock, T.W., Marioni, J.C., Gurdon, J.B., Simons, B.D., Jullien, J., 2019. Identification of a regeneration-organizing cell in the *Xenopus* tail. Science 364, 653–658. https://doi.org/10.1126/science.aav9996

Becht, E., McInnes, L., Healy, J., Dutertre, C.-A., Kwok, I.W.H., Ng, L.G., Ginhoux, F., Newell, E.W., 2019. Dimensionality reduction for visualizing single-cell data using UMAP. Nature Biotechnology 37, 38–44. https://doi.org/10.1038/nbt.4314

Beck, C.W., Christen, B., Barker, D., Slack, J.M.W., 2006. Temporal requirement for bone morphogenetic proteins in regeneration of the tail and limb of Xenopus tadpoles. Mechanisms of Development 123, 674–688. https://doi.org/10.1016/j.mod.2006.07.001

Beck, C.W., Izpisúa Belmonte, J.C., Christen, B., 2009. Beyond early development: *Xenopus* as an emerging model for the study of regenerative mechanisms. Dev. Dyn. 238, 1226–1248. https://doi.org/10.1002/dvdy.21890

Boehm, B., Westerberg, H., Lesnicar-Pucko, G., Raja, S., Rautschka, M., Cotterell, J., Swoger, J., Sharpe, J., 2010. The Role of Spatially Controlled Cell Proliferation in Limb Bud Morphogenesis. PLoS Biol 8, e1000420. https://doi.org/10.1371/journal.pbio.1000420

Butler, A., Hoffman, P., Smibert, P., Papalexi, E., Satija, R., 2018. Integrating single-cell transcriptomic data across different conditions, technologies, and species. Nature Biotechnology 36, 411–420. https://doi.org/10.1038/nbt.4096

Butler, E.G., 1955. Regeneration of the urodele forelimb after reversal of its proximo-distal axis. Journal of Morphology 96, 265–281. https://doi.org/10.1002/jmor.1050960204

Campbell, L.J., Crews, C.M., 2008. Molecular and Cellular Basis of Regeneration and Tissue Repair: Wound epidermis formation and function in urodele amphibian limb regeneration. Cell. Mol. Life Sci. 65, 73–79. https://doi.org/10.1007/s00018-007-7433-z

Campbell, L.J., Suárez-Castillo, E.C., Ortiz-Zuazaga, H., Knapp, D., Tanaka, E.M., Crews, C.M., 2011. Gene expression profile of the regeneration epithelium during axolotl limb regeneration. Developmental Dynamics 240, 1826–1840. https://doi.org/10.1002/dvdy.22669

Cannata, S.M., Bernardini, S., Filoni, S., 1992. Regenerative responses in cultured hindlimb stumps of larvalXenopus laevis. J. Exp. Zool. 262, 446–453. https://doi.org/10.1002/jez.1402620412

Choi, H.M.T., Beck, V.A., Pierce, N.A., 2014. Next-Generation in Situ Hybridization Chain Reaction: Higher Gain, Lower Cost, Greater Durability. ACS Nano 8, 4284–4294. https://doi.org/10.1021/nn405717p

Choi, H.M.T., Schwarzkopf, M., Fornace, M.E., Acharya, A., Artavanis, G., Stegmaier, J., Cunha, A., Pierce, N.A., 2018. Third-generation in situ hybridization chain reaction: multiplexed, quantitative, sensitive, versatile, robust. Development 145. https://doi.org/10.1242/dev.165753

Christen, B., Slack, J.M.W., 1997. FGF-8Is Associated with Anteroposterior Patterning and Limb Regeneration inXenopus. Developmental Biology 192, 455–466. https://doi.org/10.1006/dbio.1997.8732

Christensen, R.N., Tassava, R.A., 2000. Apical epithelial cap morphology and fibronectin gene expression in regenerating axolotl limbs. Developmental Dynamics 217, 216–224. https://doi.org/10.1002/(SICI)1097-0177(200002)217:2<216::AID-DVDY8>3.0.CO;2-8

Dent, J.N., 1962. Limb regeneration in larvae and metamorphosing individuals of the South African clawed toad. J. Morphol. 110, 61–77. https://doi.org/10.1002/jmor.1051100105

D'Jamoos, C.A., McMahon, G., Tsonis, P.A., 1998. Fibroblast growth factor receptors regulate the ability for hindlimb regeneration in Xenopus laevis. Wound Repair Regen 6, S-388-S-397. https://doi.org/10.1046/j.1460-9568.1998.60415.x

Gerber, T., Murawala, P., Knapp, D., Masselink, W., Schuez, M., Hermann, S., Gac-Santel, M., Nowoshilow, S., Kageyama, J., Khattak, S., Currie, J.D., Camp, J.G., Tanaka, E.M., Treutlein, B., 2018. Single-cell analysis uncovers convergence of cell identities during axolotl limb regeneration. Science 362, eaaq0681. https://doi.org/10.1126/science.aaq0681

Ghosh, S., Roy, S., Séguin, C., Bryant, S.V., Gardiner, D.M., 2008. Analysis of the expression and function of Wnt-5a and Wnt-5b in developing and regenerating axolotl

(Ambystoma mexicanum) limbs. Development, Growth & Differentiation 50, 289–297. https://doi.org/10.1111/j.1440-169X.2008.01000.x

Haas, B.J., Whited, J.L., 2017. Advances in Decoding Axolotl Limb Regeneration. Trends in Genetics 33, 553–565. https://doi.org/10.1016/j.tig.2017.05.006

Han, M.-J., An, J.-Y., Kim, W.-S., 2001. Expression patterns of Fgf-8 during development and limb regeneration of the axolotl. Developmental Dynamics 220, 40–48. https://doi.org/10.1002/1097-0177(2000)9999:9999<::AID-DVDY1085>3.0.CO;2-8

Hay, E.D., Fischman, D.A., 1961. Origin of the blastema in regenerating limbs of the newt Triturus viridescens. An autoradiographic study using tritiated thymidine to follow cell proliferation and migration. Dev Biol 3, 26–59. https://doi.org/10.1016/0012-1606(61)90009-4

Higher Vertebrates Do Not Regenerate Digits and Legs Because the Wound Epidermis Is Not Functional - TASSAVA - 1982 - Differentiation - Wiley Online Library [WWW Document], n.d. URL https://onlinelibrary.wiley.com/doi/epdf/10.1111/j.1432-0436.1982.tb01242.x (accessed 4.26.20).

Hutchison, C., Pilote, M., Roy, S., 2007. The axolotl limb: A model for bone development, regeneration and fracture healing. Bone 40, 45–56. https://doi.org/10.1016/j.bone.2006.07.005

Jones, T.E.M., Day, R.C., Beck, C.W., 2013. Attenuation of bone morphogenetic protein signaling during amphibian limb development results in the generation of stage-specific defects. J. Anat. n/a-n/a. https://doi.org/10.1111/joa.12098

Kato, T., Miyazaki, K., Shimizu-Nishikawa, K., Koshiba, K., Obara, M., Mishima, H.K., Yoshizato, K., 2003. Unique expression patterns of matrix metalloproteinases in regenerating newt limbs. Dev Dyn 226, 366–376. https://doi.org/10.1002/dvdy.10247

Kelley, R.O., Fallon, J.F., 1976. Ultrastructural analysis of the apical ectodermal ridge during vertebrate limb morphogenesis: I. The human forelimb with special reference to gap junctions. Developmental Biology 51, 241–256. https://doi.org/10.1016/0012-1606(76)90141-X

Knapp, D., Schulz, H., Rascon, C.A., Volkmer, M., Scholz, J., Nacu, E., Le, M., Novozhilov, S., Tazaki, A., Protze, S., Jacob, T., Hubner, N., Habermann, B., Tanaka, E.M., 2013. Comparative Transcriptional Profiling of the Axolotl Limb Identifies a Tripartite Regeneration-Specific Gene Program. PLOS ONE 8, e61352. https://doi.org/10.1371/journal.pone.0061352

Leigh, N.D., Dunlap, G.S., Johnson, K., Mariano, R., Oshiro, R., Wong, A.Y., Bryant, D.M., Miller, B.M., Ratner, A., Chen, A., Ye, W.W., Haas, B.J., Whited, J.L., 2018. Transcriptomic landscape of the blastema niche in regenerating adult axolotl limbs at single-cell resolution. Nat Commun 9, 5153. https://doi.org/10.1038/s41467-018-07604-0

Li, H., Wei, X., Zhou, L., Zhang, W., Wang, Chen, Guo, Y., Li, D., Chen, J., Liu, T., Zhang, Y., Ma, S., Wang, Congyan, Tan, F., Xu, J., Liu, Y., Yuan, Y., Chen, L., Wang, Q., Qu, J., Shen, Y., Liu, S., Fan, G., Liu, L., Liu, X., Hou, Y., Liu, G.-H., Gu, Y., Xu, X., 2020. Dynamic cell transition and immune response landscapes of axolotl limb regeneration revealed by single-cell analysis. Protein Cell. https://doi.org/10.1007/s13238-020-00763-1

Mescher, A.L., 1976. Effects on adult newt limb regeneration of partial and complete skin flaps over the amputation surface. Journal of Experimental Zoology 195, 117–127. https://doi.org/10.1002/jez.1401950111

Miyazaki, K., Uchiyama, K., Imokawa, Y., Yoshizato, K., 1996. Cloning and characterization of cDNAs for matrix metalloproteinases of regenerating newt limbs. PNAS 93, 6819–6824. https://doi.org/10.1073/pnas.93.13.6819

Monaghan, J.R., Athippozhy, A., Seifert, A.W., Putta, S., Stromberg, A.J., Maden, M., Gardiner, D.M., Voss, S.R., 2012. Gene expression patterns specific to the regenerating limb of the Mexican axolotl. Biology Open 1, 937–948. https://doi.org/10.1242/bio.20121594

Nacu, E., Gromberg, E., Oliveira, C.R., Drechsel, D., Tanaka, E.M., 2016. FGF8 and SHH substitute for anterior–posterior tissue interactions to induce limb regeneration. Nature 533, 407–410. https://doi.org/10.1038/nature17972

Nacu, E., Tanaka, E.M., 2011. Limb Regeneration: A New Development? Annual Review of Cell and Developmental Biology 27, 409–440. https://doi.org/10.1146/annurev-cellbio-092910-154115

Nieuwkoop, P.D., Faber, J., 1994. Normal Table of Xenopus Laevis (Daudin): A Systematical and Chronological Survey of the Development from the Fertilized Egg Till the End of Metamorphosis. Garland Pub.

Nye, H.L.D., Cameron, J.A., 2005. Strategies to reduce variation inXenopus regeneration studies. Dev. Dyn. 234, 151–158. https://doi.org/10.1002/dvdy.20508

Pajni-Underwood, S., Wilson, C.P., Elder, C., Mishina, Y., Lewandoski, M., 2007. BMP signals control limb bud interdigital programmed cell death by regulating FGF signaling. Development 134, 2359–2368. https://doi.org/10.1242/dev.001677

Pearl, E.J., Barker, D., Day, R.C., Beck, C.W., 2008. Identification of genes associated with regenerative success of Xenopus laevis hindlimbs. BMC Dev Biol 8, 66. https://doi.org/10.1186/1471-213X-8-66

Pizette, S., Abate-Shen, C., Niswander, L., 2001. BMP links limb growth and dorsoventral patterning. Development 4463–4474.

Pizette, S., Niswander, L., 1999. BMPs negatively regulate structure and function of the limb apical ectodermal ridge. Development 883–894.

Purushothaman, S., Elewa, A., Seifert, A.W., 2019. Fgf-signaling is compartmentalized within the mesenchyme and controls proliferation during salamander limb development. eLife 8, e48507. https://doi.org/10.7554/eLife.48507

Qin, T., Fan, C.-M., Wang, T.-Z., Sun, H., Zhao, Y.-Y., Yan, R.-J., Yang, L., Shen, W.-L., Lin, J.-X., Bunpetch, V., Cucchiarini, M., Clement, N.D., Mason, C.E., Nakamura, N., Bhonde, R., Yin, Z., Chen, X., 2020. Single-cell RNA-seq reveals novel mitochondria-related musculoskeletal cell populations during adult axolotl limb regeneration process. Cell Death Differ. https://doi.org/10.1038/s41418-020-00640-8

Rodgers, A.K., Smith, J.J., Voss, S.R., 2020. Identification of immune and non-immune cells in regenerating axolotl limbs by single-cell sequencing. Experimental Cell Research 394, 112149. https://doi.org/10.1016/j.yexcr.2020.112149

Sessions, S.K., Bryant, S.V., 1988. Evidence that regenerative ability is an intrinsic property of limb cells inXenopus. J. Exp. Zool. 247, 39–44. https://doi.org/10.1002/jez.1402470106

Shibata, E., Yokota, Y., Horita, N., Kudo, A., Abe, G., Kawakami, K., Kawakami, A., 2016. Fgf signalling controls diverse aspects of fin regeneration. Development 143, 2920–2929. https://doi.org/10.1242/dev.140699

Stocum, D.L., 1981. Distal transformation in regenerating double anterior axolotl limbs. Development 65, 3–18.

Storer, M., Mas, A., Robert-Moreno, A., Pecoraro, M., Ortells, M.C., Di Giacomo, V., Yosef, R., Pilpel, N., Krizhanovsky, V., Sharpe, J., Keyes, W.M., 2013. Senescence Is a Developmental Mechanism that Contributes to Embryonic Growth and Patterning. Cell 155, 1119–1130. https://doi.org/10.1016/j.cell.2013.10.041

Storer, M.A., Mahmud, N., Karamboulas, K., Borrett, M.J., Yuzwa, S.A., Gont, A., Androschuk, A., Sefton, M.V., Kaplan, D.R., Miller, F.D., 2020. Acquisition of a Unique Mesenchymal Precursor-like Blastema State Underlies Successful Adult Mammalian Digit Tip Regeneration. Developmental Cell 52, 509-524.e9. https://doi.org/10.1016/j.devcel.2019.12.004

Tassava, R.A., Loyd, R.M., 1977. Injury requirement for initiation of regeneration of newt limbs which have whole skin grafts. Nature 268, 49–50. https://doi.org/10.1038/268049a0

Tassava, R.A., Mescher, A.L., 1975. The Roles of Injury, Nerves, and the Wound Epidermis during the Initiation of Amphibian Limb Regeneration. Differentiation 4, 23–24. https://doi.org/10.1111/j.1432-0436.1975.tb01439.x

Thornton, C.S., 1960. Influence of an eccentric epidermal cap on limb regeneration in Amblystoma larvae. Developmental Biology 2, 551–569. https://doi.org/10.1016/0012-1606(60)90054-3

Thornton, C.S., Thornton, M.T., 1965. The regeneration of accessory limb parts following epidermal cap transplantation in urodeles. Experientia 21, 146–148. https://doi.org/10.1007/BF02141984

Tsai, S.L., Baselga-Garriga, C., Melton, D.A., 2020. Midkine is a dual regulator of wound epidermis development and inflammation during the initiation of limb regeneration. eLife 9, e50765. https://doi.org/10.7554/eLife.50765

Tsai, S.L., Baselga-Garriga, C., Melton, D.A., 2019. Blastemal progenitors modulate immune signaling during early limb regeneration. Development 146, dev169128. https://doi.org/10.1242/dev.169128

Verheyden, J.M., Sun, X., 2008. An Fgf/Gremlin inhibitory feedback loop triggers termination of limb bud outgrowth. Nature 454, 638–641. https://doi.org/10.1038/nature07085

Vincent, E., Villiard, E., Sader, F., Dhakal, S., Kwok, B.H., Roy, S., 2020. BMP signaling is essential for sustaining proximo-distal progression in regenerating axolotl limbs. Development 147, dev170829. https://doi.org/10.1242/dev.170829

Vortkamp, A., Pathi, S., Peretti, G.M., Caruso, E.M., Zaleske, D.J., Tabin, C.J., 1998. Recapitulation of signals regulating embryonic bone formation during postnatal growth and in fracture repair. Mech Dev 71, 65–76. https://doi.org/10.1016/s0925-4773(97)00203-7

Wang, C.-K.L., Omi, M., Ferrari, D., Cheng, H.-C., Lizarraga, G., Chin, H.-J., Upholt, W.B., Dealy, C.N., Kosher, R.A., 2004. Function of BMPs in the apical ectoderm of the developing mouse limb. Developmental Biology 269, 109–122. https://doi.org/10.1016/j.ydbio.2004.01.016

Wolfe, A.D., Nye, H.L., Cameron, J.A., 2000. Extent of ossification at the amputation plane is correlated with the decline of blastema formation and regeneration in Xenopus laevis hindlimbs. Dev Dyn 218, 681–697. https://doi.org/10.1002/1097-0177(2000)9999:9999<::AID-DVDY1018>3.0.CO;2-6

Wolfe, A.D., Nye, H.L.D., Cameron, J.A., n.d. Extent of ossification at the amputation plane is correlated with the decline of blastema formation and regeneration in Xenopus laevis hindlimbs 17.

Yang, E.V., Gardiner, D.M., Carlson, M.R., Nugas, C.A., Bryant, S.V., 1999. Expression of Mmp-9 and related matrix metalloproteinase genes during axolotl limb regeneration. Dev Dyn 216, 2–9. https://doi.org/10.1002/(SICI)1097-0177(199909)216:1<2::AID-DVDY2>3.0.CO;2-P

Yokoyama, H., Ide, H., Tamura, K., 2001. FGF-10 Stimulates Limb Regeneration Ability in Xenopus laevis. Developmental Biology 233, 72–79. https://doi.org/10.1006/dbio.2001.0180

Yokoyama, H., Maruoka, T., Ochi, H., Aruga, A., Ohgo, S., Ogino, H., Tamura, K., 2011. Different Requirement for Wnt/β-Catenin Signaling in Limb Regeneration of Larval and Adult Xenopus. PLoS ONE 6, e21721. https://doi.org/10.1371/journal.pone.0021721

Yokoyama, H., Yonei-Tamura, S., Endo, T., Izpisúa Belmonte, J.C., Tamura, K., Ide, H., 2000. Mesenchyme with fgf-10 Expression Is Responsible for Regenerative Capacity in Xenopus Limb Buds. Developmental Biology 219, 18–29. https://doi.org/10.1006/dbio.1999.9587

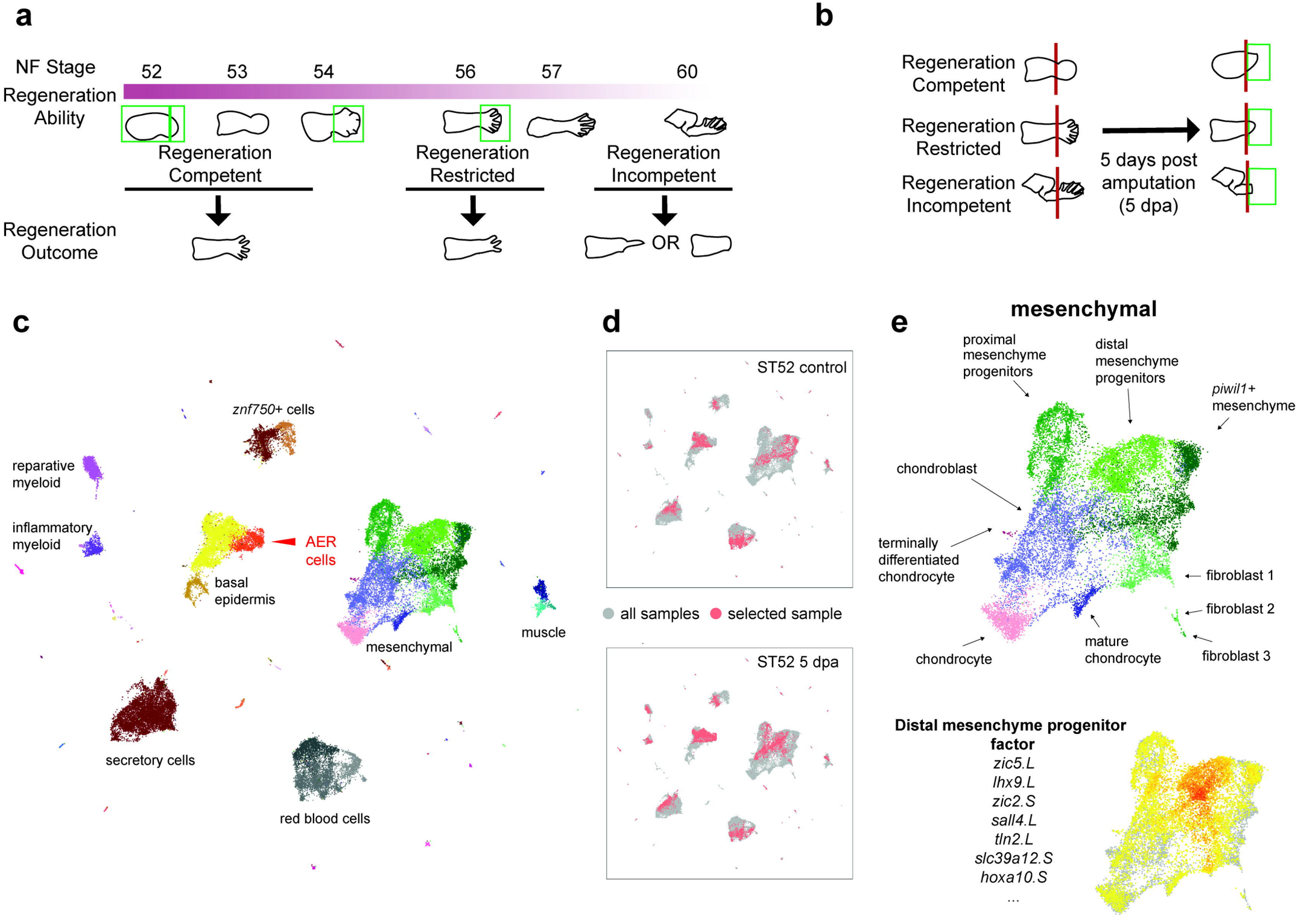
a
NF Stage
52
53
54
56
57
60
Regeneration Ability
Regeneration Competent
Regeneration Restricted
Regeneration Incompetent
Regeneration Outcome
OR
b
Regeneration Competent
Regeneration Restricted
Regeneration Incompetent
5 days post amputation (5 dpa)
c
znf750+ cells
reparative myeloid
inflammatory myeloid
AER cells
basal epidermis
mesenchymal
muscle
secretory cells
red blood cells
d
ST52 control
all samples
selected sample
ST52 5 dpa
e
mesenchymal
proximal mesenchyme progenitors
distal mesenchyme progenitors
piwil1+ mesenchyme
chondroblast
terminally differentiated chondrocyte
fibroblast 1
fibroblast 2
fibroblast 3
chondrocyte
mature chondrocyte
Distal mesenchyme progenitor factor
zic5.L
lhx9.L
zic2.S
sall4.L
tln2.L
slc39a12.S
hoxa10.S
...

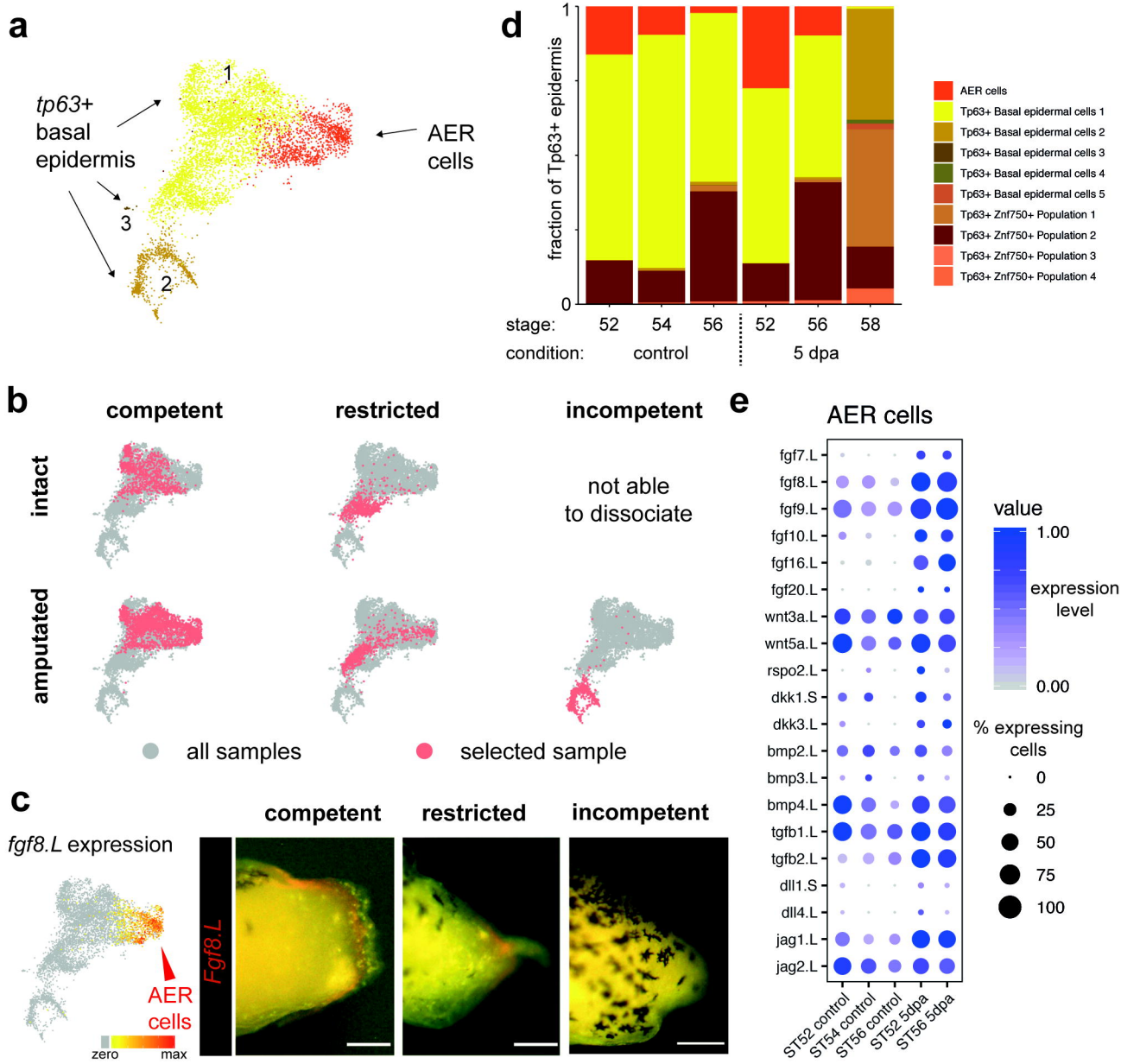
a
tp63+
basal
epidermis
AER
cells
1
2
3
d
fraction of Tp63+ epidermis
1
0
stage:
52
54
56
52
56
58
condition:
control
5 dpa
AER cells
Tp63+ Basal epidermal cells 1
Tp63+ Basal epidermal cells 2
Tp63+ Basal epidermal cells 3
Tp63+ Basal epidermal cells 4
Tp63+ Basal epidermal cells 5
Tp63+ Znf750+ Population 1
Tp63+ Znf750+ Population 2
Tp63+ Znf750+ Population 3
Tp63+ Znf750+ Population 4
b
competent
restricted
incompetent
intact
amputated
not able
to dissociate
all samples
selected sample
e
AER cells
fgf7.L
fgf8.L
fgf9.L
fgf10.L
fgf16.L
fgf20.L
wnt3a.L
wnt5a.L
rspo2.L
dkk1.S
dkk3.L
bmp2.L
bmp3.L
bmp4.L
tgfb1.L
tgfb2.L
dll1.S
dll4.L
jag1.L
jag2.L
ST52 control
ST54 control
ST56 control
ST52 5dpa
ST56 5dpa
value
1.00
expression
level
0.00
% expressing
cells
0
25
50
75
100
c
fgf8.L expression
AER
cells
zero
max
competent
restricted
incompetent
Fgf8.L

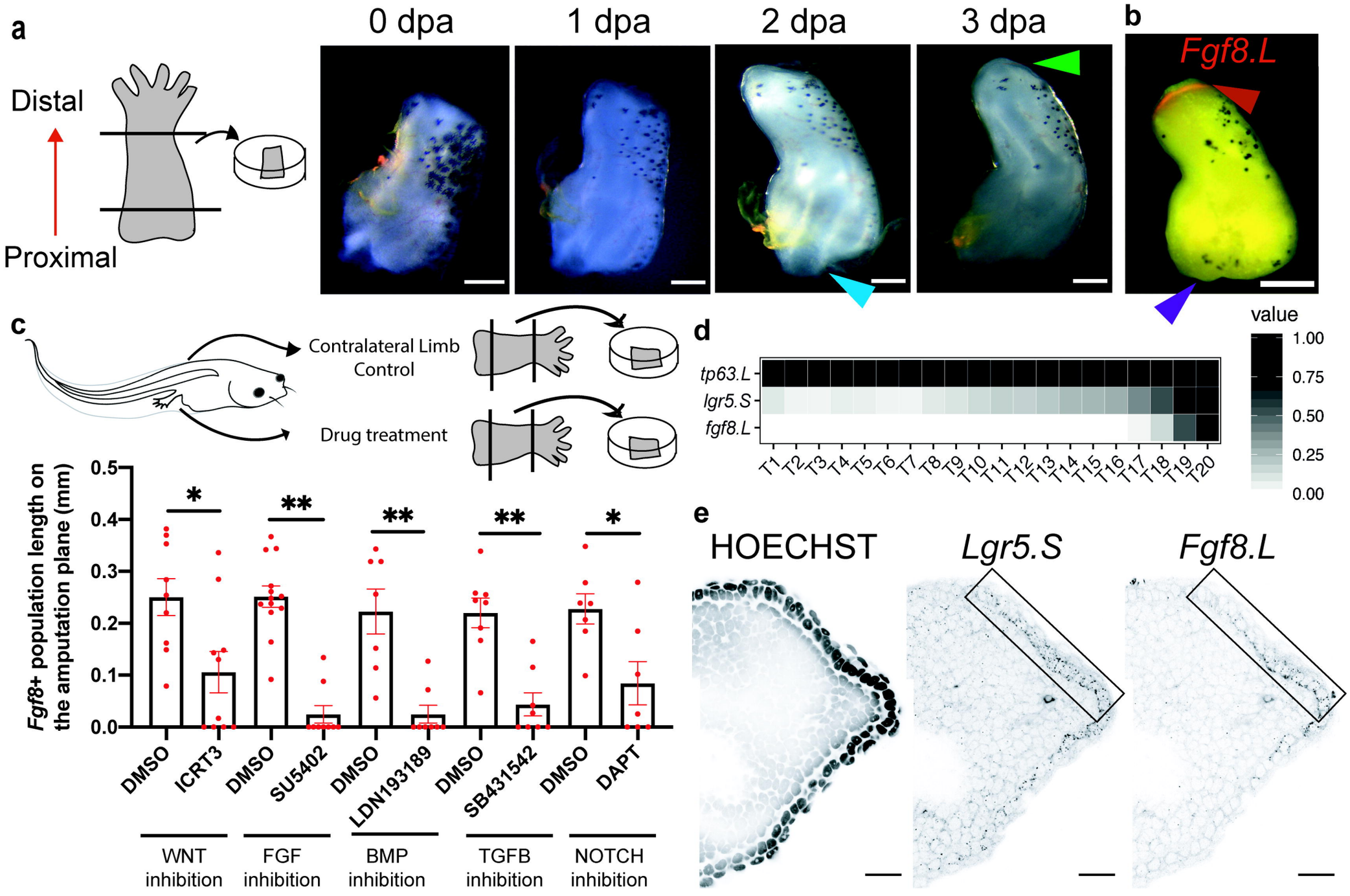
a
Distal
Proximal
0 dpa
1 dpa
2 dpa
3 dpa
b
Fgf8.L
c
Contralateral Limb
Control
Drug treatment
d
value
1.00
0.75
0.50
0.25
0.00
tp63.L
lgr5.S
fgf8.L
T1
T2
T3
T4
T5
T6
T7
T8
T9
T10
T11
T12
T13
T14
T15
T16
T17
T18
T19
T20
Fgf8+ population length on the amputation plane (mm)
0.5
0.4
0.3
0.2
0.1
0.0
*
**
**
**
*
DMSO
ICRT3
DMSO
SU5402
DMSO
LDN193189
DMSO
SB431542
DMSO
DAPT
WNT inhibition
FGF inhibition
BMP inhibition
TGFB inhibition
NOTCH inhibition
e
HOECHST
Lgr5.S
Fgf8.L
Lgr5.S
Fgf8.L

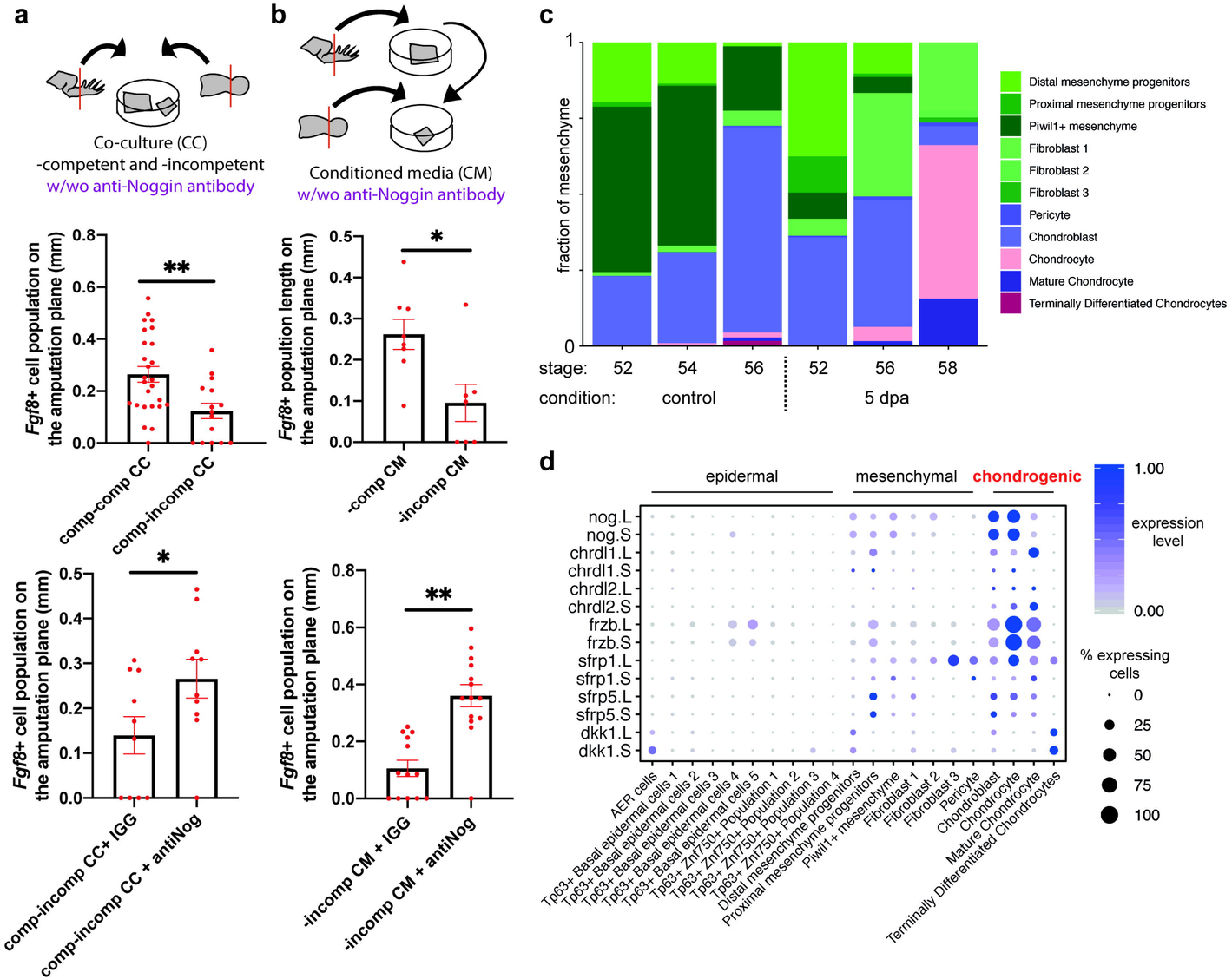
a
Co-culture (CC)
-competent and -incompetent
w/wo anti-Noggin antibody
b
Conditioned media (CM)
w/wo anti-Noggin antibody
Fgf8+ cell population on the amputation plane (mm)
**
comp-comp CC
comp-incomp CC
Fgf8+ popultion length on the amputation plane (mm)
*
-comp CM
-incomp CM
*
comp-incomp CC+ IGG
comp-incomp CC + antiNog
**
-incomp CM + IGG
-incomp CM + antiNog
c
fraction of mesenchyme
Distal mesenchyme progenitors
Proximal mesenchyme progenitors
Piwil1+ mesenchyme
Fibroblast 1
Fibroblast 2
Fibroblast 3
Pericyte
Chondroblast
Chondrocyte
Mature Chondrocyte
Terminally Differentiated Chondrocytes
stage: 52 54 56 52 56 58
condition: control 5 dpa
d
epidermal
mesenchymal
chondrogenic
nog.L
nog.S
chrdl1.L
chrdl1.S
chrdl2.L
chrdl2.S
frzb.L
frzb.S
sfrp1.L
sfrp1.S
sfrp5.L
sfrp5.S
dkk1.L
dkk1.S
AER cells
Tp63+ Basal epidermal cells 1
Tp63+ Basal epidermal cells 2
Tp63+ Basal epidermal cells 3
Tp63+ Basal epidermal cells 4
Tp63+ Basal epidermal cells 5
Tp63+ Znf750+ Population 1
Tp63+ Znf750+ Population 2
Tp63+ Znf750+ Population 3
Tp63+ Znf750+ Population 4
Distal mesenchyme progenitors
Proximal mesenchyme progenitors
Piwil1+ mesenchyme
Fibroblast 1
Fibroblast 2
Fibroblast 3
Pericyte
Chondroblast
Chondrocyte
Mature Chondrocyte
Terminally Differentiated Chondrocytes
1.00
expression level
0.00
% expressing cells
0
25
50
75
100

a

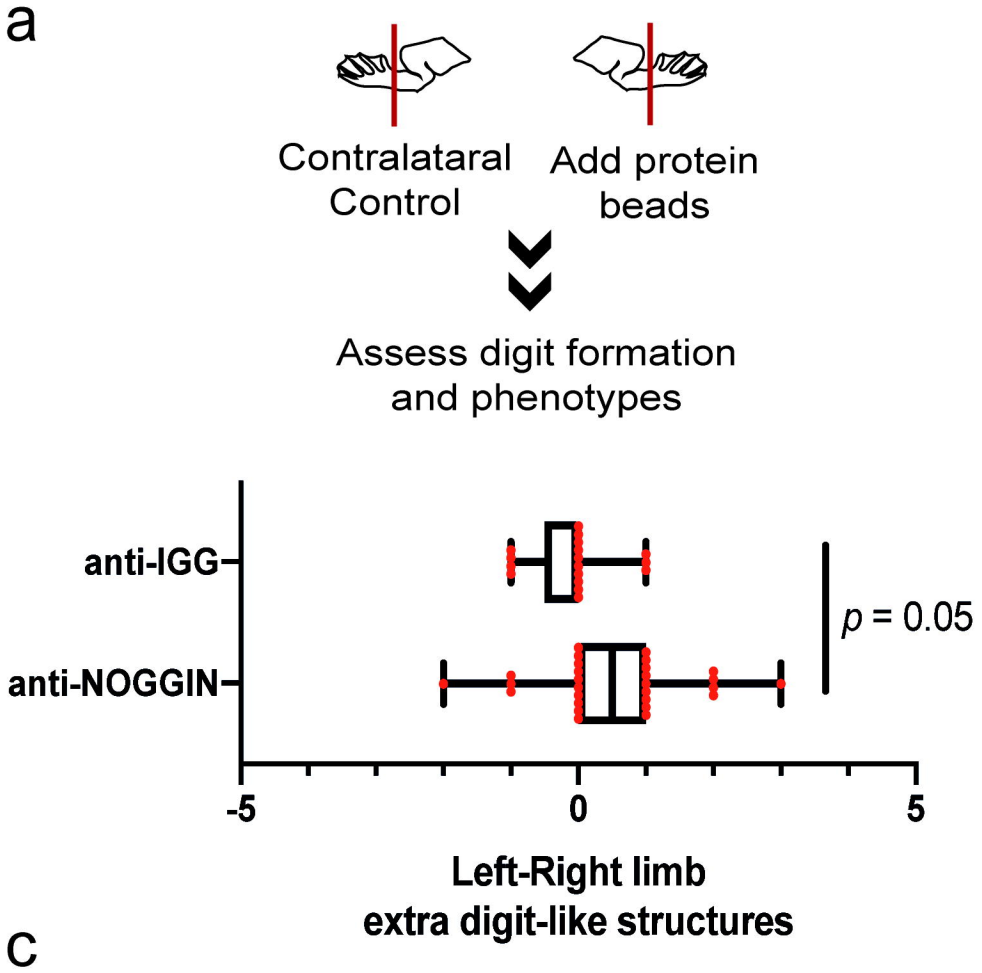
Contralataral Control
Add protein beads
Assess digit formation and phenotypes
anti-IGG
anti-NOGGIN
p = 0.05
-5
0
5
Left-Right limb extra digit-like structures

b

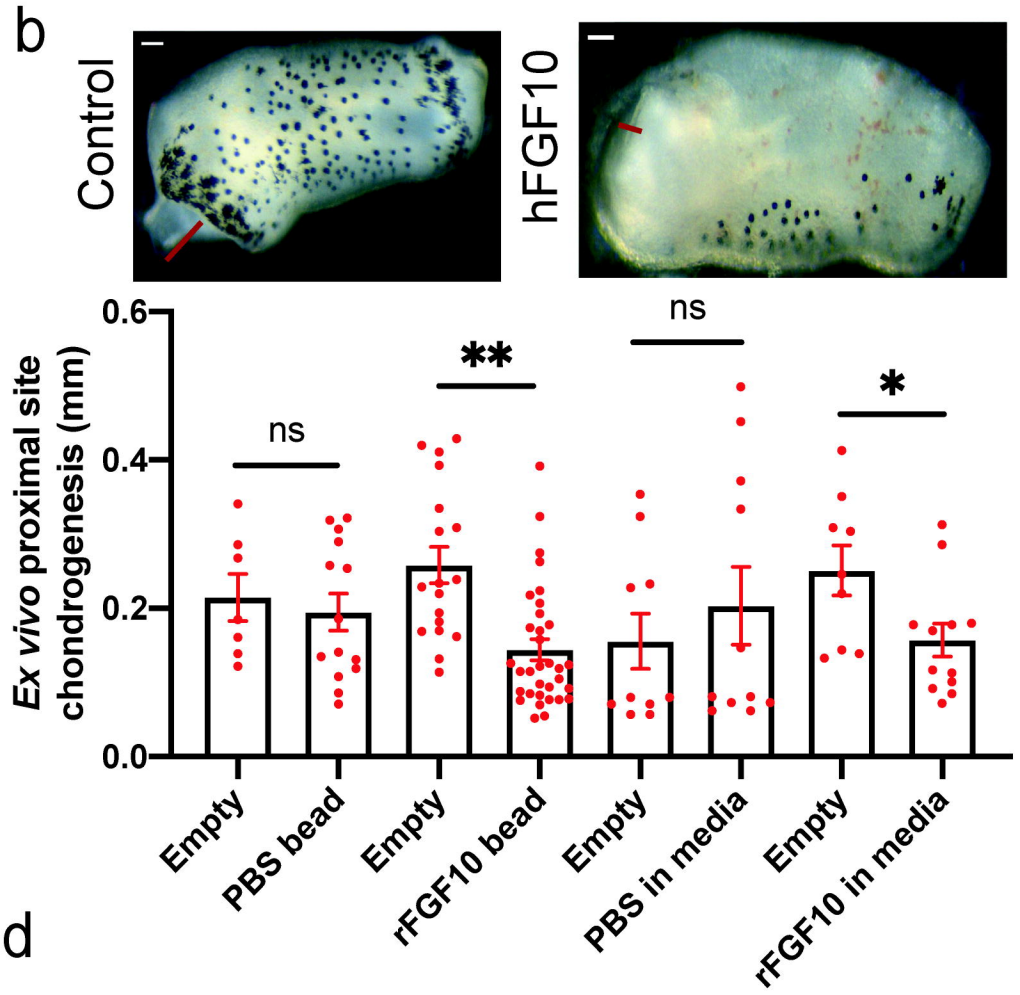
Control
hFGF10
Ex vivo proximal site chondrogenesis (mm)
0.0
0.2
0.4
0.6
ns
**
ns
*
Empty
PBS bead
Empty
rFGF10 bead
Empty
PBS in media
Empty
rFGF10 in media

c

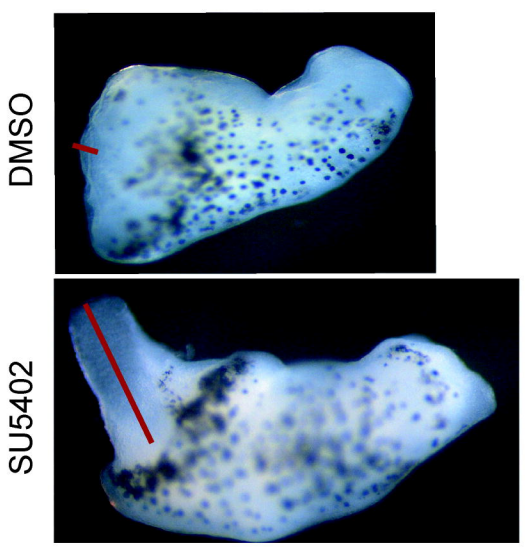
DMSO
SU5402

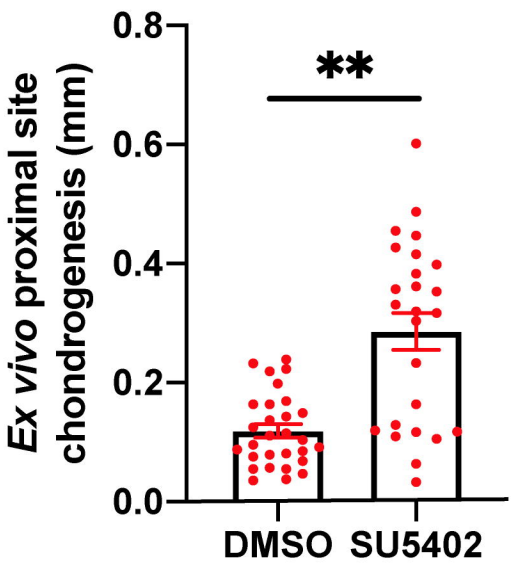
Ex vivo proximal site chondrogenesis (mm)
0.0
0.2
0.4
0.6
0.8
**
DMSO
SU5402

d

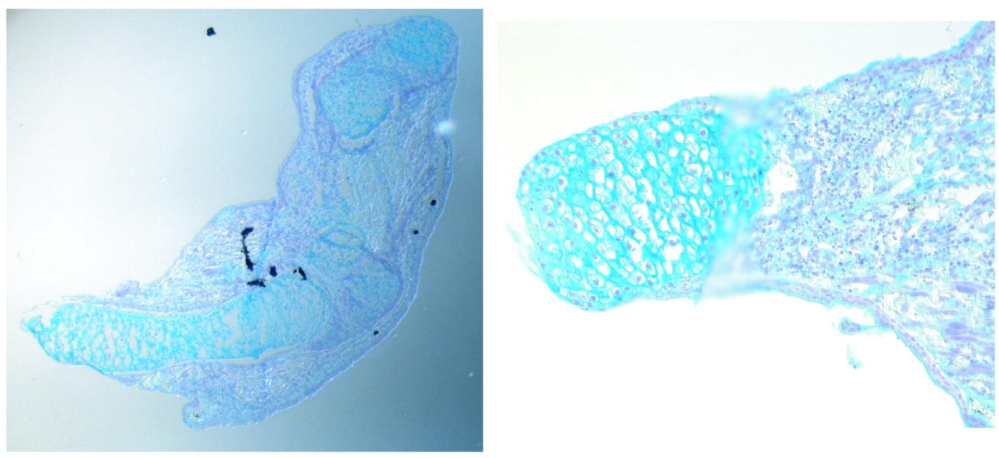

e

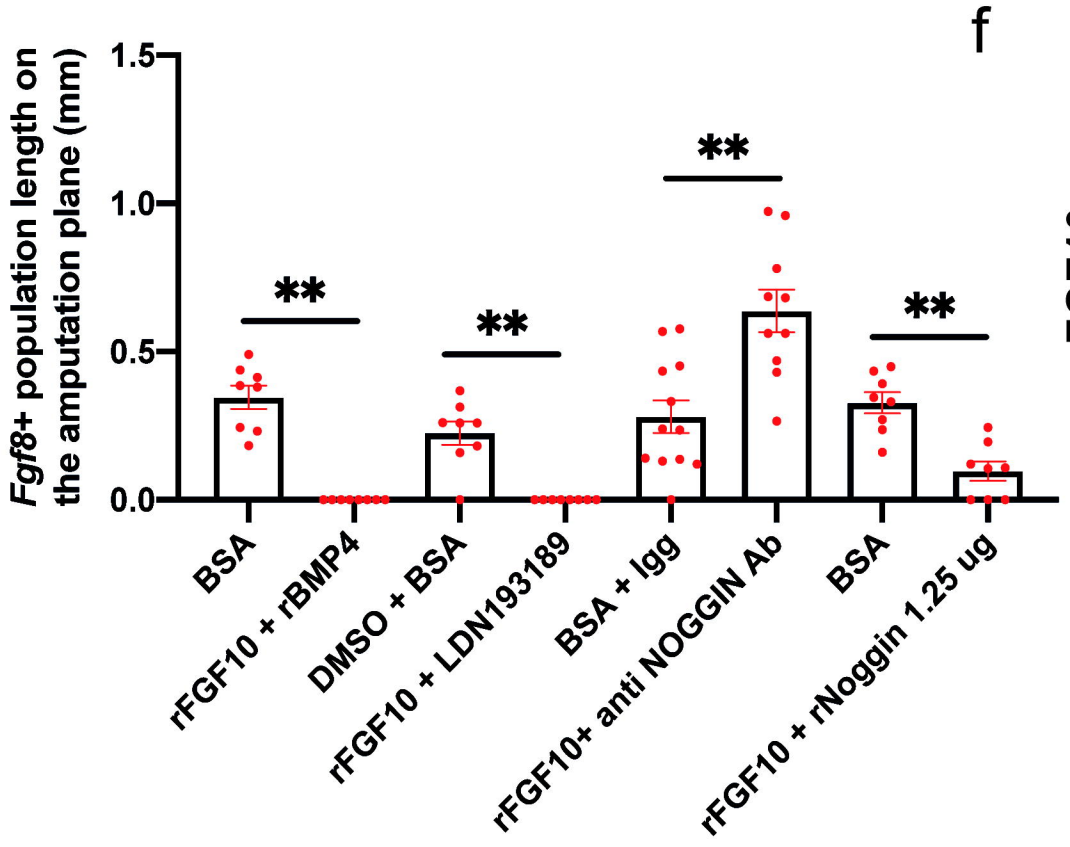
Fgf8+ population length on the amputation plane (mm)
0.0
0.5
1.0
1.5
**
**
**
**
BSA
rFGF10 + rBMP4
DMSO + BSA
rFGF10 + LDN193189
BSA + Igg
rFGF10+ anti NOGGIN Ab
BSA
rFGF10 + rNoggin 1.25 ug

f

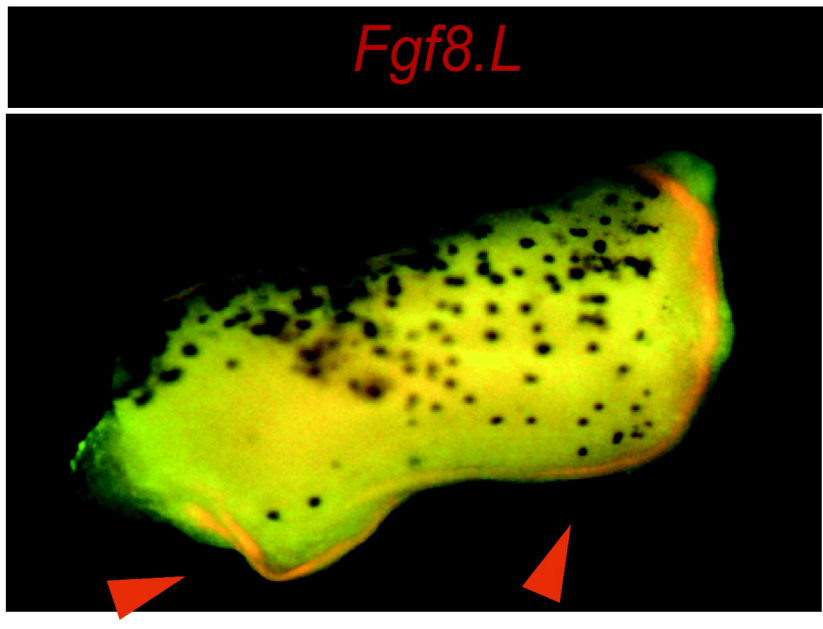
Fgf8.L
rFGF10 + anti-NOGGIN Ab

g

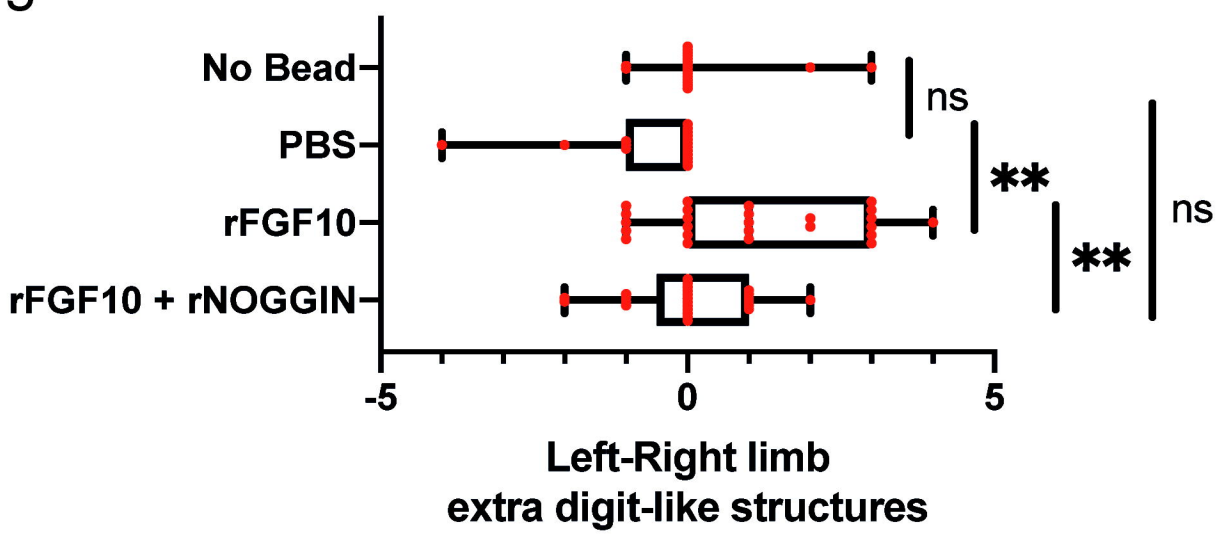
No Bead
PBS
rFGF10
rFGF10 + rNOGGIN
ns
**
**
ns
-5
0
5
Left-Right limb extra digit-like structures

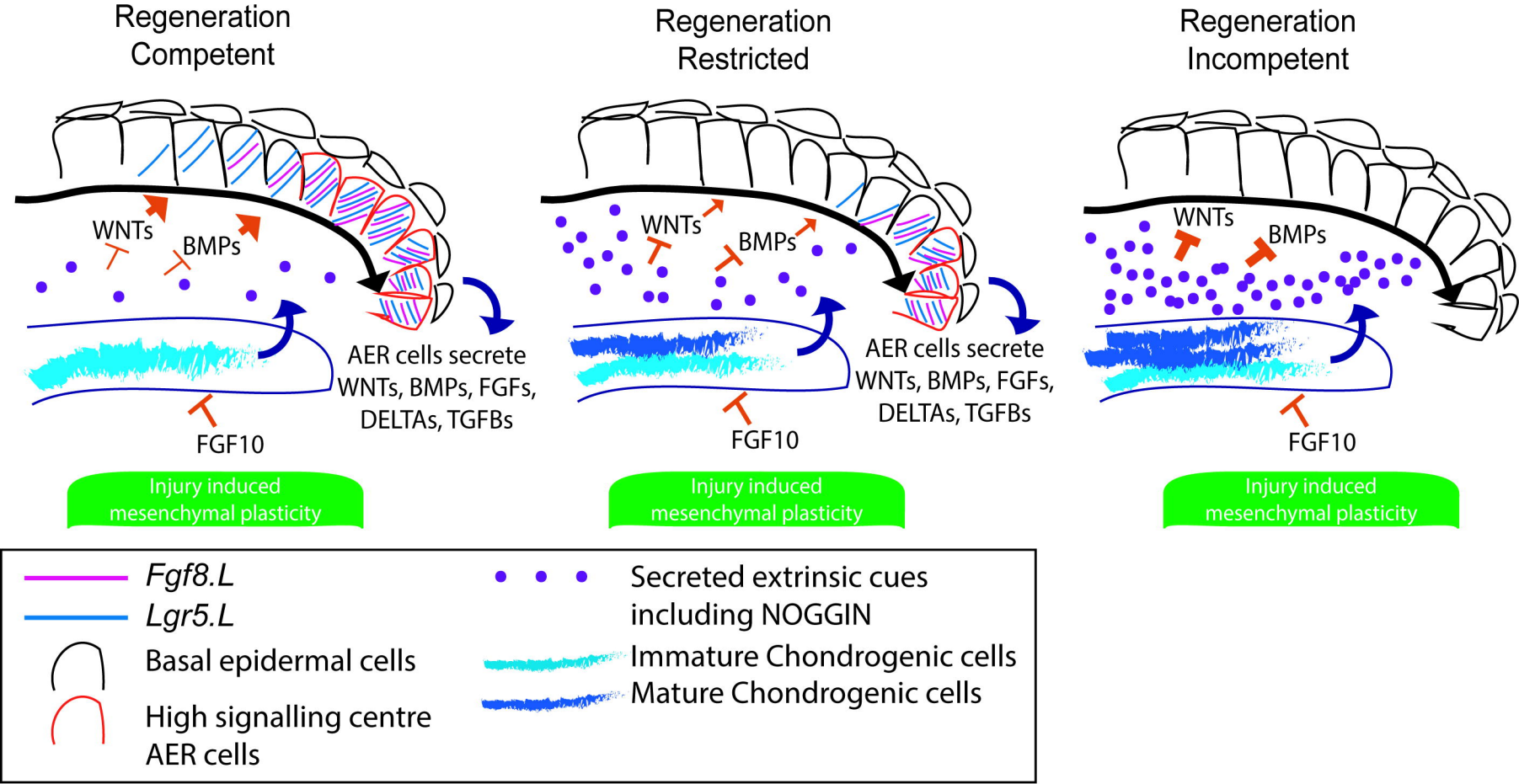
Regeneration Competent
WNTs
BMPs
AER cells secrete WNTs, BMPs, FGFs, DELTAs, TGFBs
FGF10
Injury induced mesenchymal plasticity
Regeneration Restricted
WNTs
BMPs
AER cells secrete WNTs, BMPs, FGFs, DELTAs, TGFBs
FGF10
Injury induced mesenchymal plasticity
Regeneration Incompetent
WNTs
BMPs
FGF10
Injury induced mesenchymal plasticity
Fgf8.L
Lgr5.L
Basal epidermal cells
High signalling centre AER cells
Secreted extrinsic cues including NOGGIN
Immature Chondrogenic cells
Mature Chondrogenic cells